Monthly Notices of the ROYAL ASTRONOMICAL SOCIETY

MNRAS **446,** 3062–3077 (2015) doi:10.1093/mnras/stu2258

A first-order secular theory for the post-Newtonian two-body problem with spin – II. A complete solution for the angular coordinates in the restricted case

Francesco Biscani[1]★ and Sante Carloni[2,3]

[1]*Max Planck Institute for Astronomy, Königstuhl 17, D-69117 Heidelberg, Germany*
[2]*Institute of Theoretical Physics, Faculty of Mathematics and Physics Charles University in Prague, V Holešovičkách 2 180 00 Praha 8, Czech Republic*
[3]*Centro Multidisciplinar de Astrofisica - CENTRA, Instituto Superior Tecnico - IST, Universidade de Lisboa - UL, Avenida Rovisco Pais 1, 1049-001 Lisboa, Portugal*

Accepted 2014 October 27. Received 2014 October 24; in original form 2014 June 20

ABSTRACT

Building on the results of a previous paper, we compute for the first time a full first-order perturbative solution for the angular coordinates in the restricted post-Newtonian two-body problem with spin. The analytical integration of the angular coordinates, based on the theory of the Weierstrassian functions, allows us to investigate thoroughly the spin–orbit and spin–spin interactions, and to derive several new results. The application of our solution to a selection of idealized physical systems of interest reveals a rich variety of dynamical behaviours driven by purely relativistic effects. In particular, we highlight a new relativistic nutational motion resulting from the combined spin–orbit and spin–spin interactions.

Key words: gravitation – relativistic processes – celestial mechanics.

1 INTRODUCTION

The problem of understanding the corrections that General Relativity imposes on Newtonian mechanics in the case of weak gravitational fields (and low velocities compared to the speed of light), also known as post-Newtonian (PN) gravitation, is one of the crucial aspects of the local testing of Einstein's theory of gravitation, and it has been a matter of research for long time. In spite of these efforts, however, our understanding of PN gravitation is still incomplete not only at high PN orders, but also in terms of its actual foundations.

In particular, the first formulation of PN gravitation, given by Lorentz and Droste (Lorentz 1937) and later by Einstein himself (Einstein, Infeld & Hoffmann 1938), has been found to present a series of shortcomings which require the reformulation of the problem in some more sophisticated versions, like the ones proposed by Damour, Soffel & Xu (1991) or by Blanchet (2006). This is particularly true when rotating objects (which we will call *spinning* objects, referring to *spin* as their proper angular momentum) are considered, because it is not straightforward to define a notion of spin which is completely consistent with Einstein's theory. One way to avoid this issue while preserving a more classical derivation of the PN equations (at least at low PN orders) is to adopt a special definition of the spin vector like the one proposed by Damour, Jaranowski & Schäfer (2008) or the one given by Wu & Xie (2010). In the following, we will also consider such definitions.

★E-mail: bluescarni@gmail.com

Regardless of the method used to arrive at the PN equations, one is always faced with a formidable system of differential equations. In recent years, researchers have frequently employed numerical approaches for the solution of the PN equations at high orders (including dissipative terms). A particular focus of this line of research is the study of chaos in spinning compact binaries (Levin 2000, 2003, 2006; Schnittman & Rasio 2001; Cornish & Levin 2002; Hartl & Buonanno 2005; Wu & Xie 2007, 2008; Mei et al. 2013; Huang, Ni & Wu 2014). In a previous work (Biscani & Carloni 2013, from now on 'Paper I'), we adopted a different approach to the problem, aiming for an *analytical* solution to the 1PN two spinning body problem. In Paper I, we obtained for the first time an exact solution of the reduced problem using a modern perturbation technique (commonly used in the field of Celestial Mechanics) based on Lie series (Hori 1966; Deprit 1969).

Based on the theory of canonical transformation, the Lie series perturbation method allows the determination of a quasi-unitary (canonical) transformation able to bring a Hamiltonian with the structure $\mathcal{H}_0 + \epsilon\mathcal{H}_1$ to a form which is easier to treat both analytically and numerically. In particular, in Paper I it was shown that it is possible to solve exactly the averaged 1PN reduced two rotating body problem in terms of Weierstrass elliptic functions.

The Weierstrassian functions are elliptic (and related) functions introduced by Karl Weierstrass at the end of the 19th century (Whittaker & Watson 1927). Weierstrass' formulation of the theory of elliptic functions is a (mathematically equivalent and lesser-known) alternative to the more commonly encountered formulation of Jacobi. Recently, the Weierstrassian formalism has been successfully

applied to dynamical studies in General Relativity (see, e.g. Hackmann et al. 2010; Scharf 2011; Gibbons & Vyska 2012).

Using the Lie series perturbation theory and the mathematics of the Weierstrassian functions, in Paper I, we carried out an initial analysis of the evolution of the spin vector and the orbital inclination of the secondary body. The aim of the present contribution is to refine and expand these results. In particular, we will first show that it is possible to simplify the result obtained in Paper I for the exact solution of the variable H. Using this new simplified solution in conjunction with the theory of the Weierstrassian functions, we will then derive an exact solution for the angular variables. In addition, we will show that our full treatment of the 1PN reduced two rotating body problem is able to uncover previously unknown additional effects due to the spin–spin and spin–orbit interactions.

With respect to numerical solutions of the relativistic equations at high PN levels, it is clear that our approach deals with a considerably simpler physical system. Our conclusions are necessarily limited to contexts in which high PN terms can be discarded and in which our idealized averaged dynamical system can be considered a good approximation of the real one. In particular, our result on the integrability of the averaged system relies crucially on the simplifications adopted in our model (for instance, the fact that $\boldsymbol{J}_2$ is a constant of motion). Because of this, we shall not discuss aspects such as the chaoticity of the motion or the dynamical consequences of energy dissipation via the emission of gravitational waves. On the other hand, as frequently done in Celestial Mechanics, our first-order results could be used as a starting point for higher order analyses – for instance, by using the resonant action-angle variables method (see Morbidelli 2002, chapter 4).

This paper is organized in the following way. Section 2 is dedicated to a summary of the basic equations, the notation and the results of Paper I. Section 3 deals with a strategy to simplify the exact solution obtained in Paper I for the normalized z component of the orbital angular momentum H. Section 4 illustrates the integration of the angular coordinates, which was not performed in Paper I. Section 5 applies the new solutions found to some (idealized) physical systems. Finally, Section 6 is dedicated to the conclusions.

2 A SUMMARY OF THE RESULTS OF PAPER I

The starting point of our analysis in Paper I was the well-known 1PN Hamiltonian of the two-body problem with spin, which, after reduction to the centre-of-mass frame, reads (Barker & O'Connell 1970, 1979; Damour 2001)

$$\mathcal{H} = \mathcal{H}_{\rm N} + \epsilon \mathcal{H}_1 . \tag{1}$$

Here, $\epsilon = 1/c^2$ is chosen as the 'smallness parameter' of our perturbation theory and

$$\mathcal{H}_{\rm N} = \frac{1}{2}\frac{\boldsymbol{J}_1^2}{I_1} + \frac{1}{2}\frac{\boldsymbol{J}_2^2}{I_2} + \frac{\boldsymbol{p}^2}{2\mu} - \frac{\mathcal{G}M\mu}{r} \tag{2}$$

is the Newtonian Hamiltonian (representing the unperturbed problem). $\mathcal{H}_1$ expands as

$$\mathcal{H}_1 = \mathcal{H}_{\rm PN} + \mathcal{H}_{\rm SO} + \mathcal{H}_{\rm SS}, \tag{3}$$

where $\mathcal{H}_{\rm PN}$ is the PN orbital Hamiltonian, $\mathcal{H}_{\rm SO}$ the spin–orbit interaction term and $\mathcal{H}_{\rm SS}$ the spin–spin interaction term.

The structure of this Hamiltonian and, above all, the nature of the spin vectors, have been a matter of debate in the past few years (see Damour et al. 2008). More recently, Wu & Xie (2010) have proposed a symplectic formulation of the spin vectors in terms of cylindrical-like coordinates. In Paper I, we followed the interpretation of Barker & O'Connell (1975, 1976, 1979) and Wex (1995) in identifying the spins $\boldsymbol{J}_i$ as the rotational angular momenta of spherical rigid bodies, so that

$$\boldsymbol{J}_i = I_i \boldsymbol{\omega}_i , \tag{4}$$

where I_i is the moment of inertia and $\boldsymbol{\omega}_i$ the rotational angular velocity vector of body i.

The reduction of the Hamiltonian (3) to the restricted case in which $m_2 \gg m_1$ and $|\boldsymbol{J}_2| \gg |\boldsymbol{J}_1|$ reads

$$\begin{aligned}
\mathcal{H}_{\rm N} &= \frac{1}{2}\frac{\boldsymbol{J}_1^2}{I_1} + \frac{\boldsymbol{p}_1^2}{2m_1} - \frac{\mathcal{G}m_1 m_2}{r}, \\
\mathcal{H}_{\rm PN} &= m_1 \left(-\frac{1}{8}\frac{\boldsymbol{p}_1^4}{m_1^4} - \frac{3}{2}\frac{\mathcal{G}m_2}{r}\frac{\boldsymbol{p}_1^2}{m_1^2} + \frac{\mathcal{G}^2 m_2^2}{2r^2} \right), \\
\mathcal{H}_{\rm SO} &= \frac{2\mathcal{G}}{r^3}\left(\frac{3}{4}\frac{m_2}{m_1}\boldsymbol{J}_1 + \boldsymbol{J}_2 \right) \cdot \left(\boldsymbol{r} \times \boldsymbol{p}_1 \right), \\
\mathcal{H}_{\rm SS} &= \frac{\mathcal{G}}{r^3}\left[3\left(\boldsymbol{J}_1 \cdot \boldsymbol{n} \right)\left(\boldsymbol{J}_2 \cdot \boldsymbol{n} \right) - \boldsymbol{J}_1 \cdot \boldsymbol{J}_2 \right],
\end{aligned} \tag{5}$$

where $\boldsymbol{J}_2$ is now considered as a constant of motion that can be dropped from $\mathcal{H}_{\rm N}$. Without loss of generality, we oriented the reference system (now centred on body 2) in such a way that the constant $\boldsymbol{J}_2$ is aligned to the positive z-axis, so that

$$\boldsymbol{J}_2 = (0, 0, J_2), \tag{6}$$

with $J_2 = |\boldsymbol{J}_2|$.

We then proceeded to express, via a canonical transformation, the restricted Hamiltonian (5) in a set of action-angle variables for the unperturbed problem consisting of the Delaunay arguments for the orbital coordinates (Morbidelli 2002) and of the Serret–Andoyer (SA) variables for the spin coordinates (Gurfil et al. 2007).

The Delaunay arguments $(L, G, H; l, g, h)$ (where capital letters indicate momenta, small capitals coordinates) can be introduced via the following standard relations:

$$\begin{aligned}
L &= \sqrt{\mathcal{G}m_2 a}, l = M, \\
G &= L\sqrt{1-e^2}, g = \omega, \\
H &= G\cos i, h = \Omega .
\end{aligned} \tag{7}$$

Here a, e, i, M, ω and Ω are the classical Keplerian orbital elements describing the trajectory of the secondary body m_1 around the primary m_2. The Keplerian elements are in turn related to the Cartesian orbital momentum $\boldsymbol{p}_1$ and position $\boldsymbol{r}$ via well-known relations (e.g. see Murray & Dermott 2000).

The SA variables describe the rotational motion of a rigid body in terms of orientation angles and rotational angular momentum. In the SA formalism, the components of $\boldsymbol{J}_1$ read

$$\boldsymbol{J}_1 = \left(\sqrt{|\boldsymbol{J}_1|^2 - J_{1,z}^2}\sin\tilde{h}, -\sqrt{|\boldsymbol{J}_1|^2 - J_{1,z}^2}\cos\tilde{h}, J_{1,z} \right). \tag{8}$$

In the SA variables set, $\left(|\boldsymbol{J}_1|, J_{1,z}\right)$ are the generalized momenta, and $\left(\tilde{g}, \tilde{h}\right)$ are the conjugate coordinates.[1] It can be helpful to think of the SA variables as the rigid-body analogues of the Delaunay variables (e.g. $\tilde{h}$ is the 'nodal angle' of the spin vector of the secondary body on the inertial reference plane). It can be shown how

[1] The $\tilde{g}$ coordinate does not appear in the Hamiltonian (5) due to the spherical symmetry of the bodies. In the SA formalism, the $\tilde{g}$ coordinate is a measure of the orientation of the body with respect to the spin vector.

Table 1. Summary and explanation of the symbolic variables appearing in the Hamiltonians (9) and (10).

Symbol	Meaning	Alternate expression
L	Normalized square root of the semimajor axis	$\sqrt{\mathcal{G}m_2 a}$
G	Norm of the orbital angular momentum $\boldsymbol{r}\times\boldsymbol{p}_1$ normalized by m_1	$L\sqrt{1-e^2}$
H	z component of the orbital angular momentum normalized by m_1	$G\cos i$
$\tilde{G}$	Norm of spin $\boldsymbol{J}_1$ normalized by m_1	$\lvert\boldsymbol{J}_1\rvert/m_1$
$\tilde{H}$	z component of spin $\boldsymbol{J}_1$ normalized by m_1	$\tilde{G}\cos I$
l	Mean anomaly	M
g	Argument of pericentre	ω
h	Longitude of the ascending node	Ω
$\tilde{h}$	Nodal angle of spin $\boldsymbol{J}_1$	–
f	True anomaly	–
$\mathcal{I}_1$	Inverse of the moment of inertia of body 1 normalized by m_1	m_1/I_1
G_{xy}	Norm of the projection of $\boldsymbol{r}\times\boldsymbol{p}_1$ on the xy plane normalized by m_1	$\sqrt{G^2-H^2}$
$\tilde{G}_{xy}$	Norm of the projection of spin $\boldsymbol{J}_1$ on the xy plane normalized by m_1	$\sqrt{\tilde{G}^2-\tilde{H}^2}$
J_2	Norm of spin $\boldsymbol{J}_2$	$\lvert\boldsymbol{J}_2\rvert$
r	Distance between body 1 and body 2	–
m_1, m_2	Masses of the two bodies	–
$\mathcal{G}$	Universal gravitational constant	–

the SA variables correspond (after a trivial canonical transformation) to the symplectic spin variables defined in Wu & Xie (2010). The correspondence is detailed in Appendix B.

After a further rescaling with respect to the mass of the secondary body m_1 (now a meaningless quantity as the secondary body is considered as a small particle), the final form of the restricted Hamiltonian (5) in Delaunay and SA variables reads

$$\mathcal{H}_{\rm N} = \frac{1}{2}\mathcal{I}_1\tilde{G}^2 - \frac{\mathcal{G}^2 m_2^2}{2L^2}, \tag{9}$$

$$\begin{aligned}\mathcal{H}_1 = &-\frac{1}{8}\frac{\mathcal{G}^4 m_2^4}{L^4} + \frac{1}{r}\frac{2\mathcal{G}^3 m_2^3}{L^2} - \frac{1}{r^2}3\mathcal{G}^2 m_2^2\\ &+\frac{\mathcal{G}}{r^3}\left\{2J_2 H + \frac{3J_2 G_{xy}^2\tilde{H}}{2G^2} + \frac{3m_2\tilde{H}H}{2} - J_2\tilde{H}\right.\\ &+\left(\frac{3m_2}{2}\tilde{G}_{xy}G_{xy} - \frac{3}{2}J_2\frac{HG_{xy}\tilde{G}_{xy}}{G^2}\right)\cos\left(\tilde{h}-h\right)\\ &+3J_2\left[-\frac{1}{2}\frac{G_{xy}^2\tilde{H}}{G^2}\cos\left(2f+2g\right)\right.\\ &-\frac{1}{4}\frac{G_{xy}\tilde{G}_{xy}}{G}\left(1-\frac{H}{G}\right)\cos\left(2f+2g+\tilde{h}-h\right)\\ &\left.\left.+\frac{1}{4}\frac{G_{xy}\tilde{G}_{xy}}{G}\left(1+\frac{H}{G}\right)\cos\left(2f+2g-\tilde{h}+h\right)\right]\right\}.\end{aligned} \tag{10}$$

For convenience, we have summarized in Table 1 the meaning of the symbolic variables appearing in the Hamiltonians (9) and (10). We have to stress how in these expressions, r, G_{xy}, $\tilde{G}_{xy}$ and f have to be regarded as implicit functions of the canonical momenta and coordinates (rather than distinct quantities).

In Paper I, we then proceeded to the application of the Lie series perturbation technique (Hori 1966; Deprit 1969), which transformed the Hamiltonians (9) and (10) into the averaged Hamiltonian

$$\mathcal{H}' = \mathcal{H}_{\rm N} + \epsilon\left(\mathcal{F}_0 + \mathcal{F}_1\cos h_*\right) + \mathcal{O}\left(\varepsilon^2\right), \tag{11}$$

where

$$\mathcal{H}_{\rm N} = \frac{1}{2}\mathcal{I}_1\tilde{G}^2 - \frac{\mathcal{G}^2 m_2^2}{2L^2}, \tag{12}$$

$$\begin{aligned}\mathcal{F}_0 = &\frac{1}{2}\frac{J_2\mathcal{G}^4\tilde{H}_* {m_2}^3}{G^3L^3} + \frac{3}{2}\frac{H^3 J_2\mathcal{G}^4 {m_2}^3}{G^5L^3} + \frac{15}{8}\frac{\mathcal{G}^4 {m_2}^4}{L^4}\\ &+\frac{3}{2}\frac{HJ_2\mathcal{G}^4 {m_2}^3}{G^3L^3} - \frac{3}{2}\frac{H^2 J_2\mathcal{G}^4\tilde{H}_* {m_2}^3}{G^5L^3} - \frac{3}{2}\frac{H^2\mathcal{G}^4 {m_2}^4}{G^3L^3}\\ &+\frac{3}{2}\frac{H\mathcal{G}^4\tilde{H}_* {m_2}^4}{G^3L^3} - 3\frac{\mathcal{G}^4 {m_2}^4}{GL^3},\end{aligned} \tag{13}$$

$$\mathcal{F}_1 = -\frac{3}{2}\frac{G_{xy}HJ_2\mathcal{G}^4\tilde{G}_{xy*} {m_2}^3}{G^5L^3} + \frac{3}{2}\frac{G_{xy}\mathcal{G}^4\tilde{G}_{xy*} {m_2}^4}{G^3L^3}, \tag{14}$$

and

$$\tilde{G}_{xy*} = \sqrt{\tilde{G}^2 - \left(\tilde{H}_* - H\right)^2}, \tag{15}$$

$$\tilde{H}_* = H + \tilde{H}, \tag{16}$$

$$h_* = h - \tilde{h}. \tag{17}$$

From equation (11) onward, it is understood (as it is common practice when working within the Lie series perturbation framework) that the symbols $\left(L, G, H, \tilde{G}, \tilde{H}\right)$ and $\left(l, g, h, \tilde{g}, \tilde{h}\right)$ refer to the *mean* momenta and coordinates (i.e. the new momenta and coordinates introduced by the averaging canonical transformation). A fundamental advantage of the Lie series perturbation method (with respect, for instance, to the earlier von Zeipel method – see von Zeipel (1916)) is that it is possible to write explicit transformation formulae between the original variables and the averaged ones. This is explained in detail, for instance, in Heimberger, Soffel & Ruder (1990) for the relativistic artificial satellite problem. Here, however, we are concerned with the secular dynamics of the system, and will thus limit ourselves to work with the averaged variables.

After discarding the terms of order $\mathcal{O}\left(\varepsilon^2\right)$, generated by the Lie series transformation, equation (11) represents the final form of the averaged Hamiltonian. Equation (11) was obtained after an additional simple linear canonical transformation reminiscent of the treatment of single-resonance dynamics in the N-body problem (see

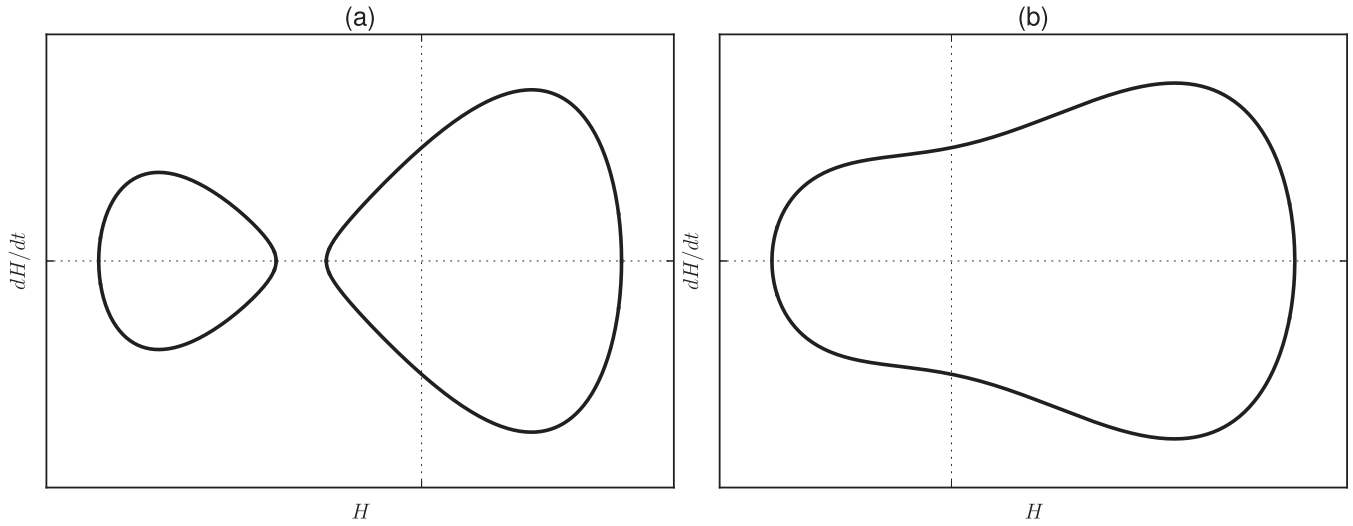

Figure 1. Representative plots of $\mathrm{d}H/\mathrm{d}t$ as a function of H as described by equation (18). In the plot on the left (a) the quartic polynomial $f_4(H)$ has four distinct real roots and the plot consists of two separate libration lobes, while in the plot on the right (b) the quartic polynomial $f_4(H)$ has two distinct real roots and the plot consists of a single libration lobe.

Lemma 4 in Morbidelli & Giorgilli 1993), in which the average generalized momenta become $\left(L, G, H, \tilde{G}, \tilde{H}_*\right)$ and the average coordinates become $\left(l, g, h_*, \tilde{g}, \tilde{h}\right)$.

The autonomous averaged Hamiltonian (11) has one degree of freedom (all momenta, apart from H, are constants of motion), and it is thus integrable in the sense of Liouville (Arnold 1989). The equation of motion for the average momentum H can be derived via Hamilton's equations in the standard way, and it can be written as

$$\frac{\mathrm{d}H}{\mathrm{d}t} = \pm\sqrt{f_4(H)}, \tag{18}$$

where $f_4(H)$ is a polynomial of degree 4 in H, whose coefficients are functions of the constants of motion and of the initial conditions of the system.

In Paper I, we showed how it is possible to integrate and invert equation (18) to yield an explicit solution for $H(t)$ via the Weierstrass elliptic functions $\wp$ and $\wp\prime$. The solution for $H(t)$ we presented in Paper I is based on a formula by Weierstrass and reported in Whittaker & Watson (1927), section 20.6, and it consists of a rather complicated rational function of $\wp$ and $\wp\prime$:

$$\begin{aligned} H(t) = H_0 + & \frac{1}{2\left[\wp(t) - \frac{1}{24}f_4''(H_0)\right]^2 - \frac{1}{48}f_4(H_0)\,f_4^{iv}(H_0)} \\ & \cdot\left\{\frac{1}{2}f_4'(H_0)\left[\wp(t) - \frac{1}{24}f_4''(H_0)\right]\right. \\ & \left. + \frac{1}{24}f_4(H_0)\,f_4'''(H_0) \pm \sqrt{f_4(H_0)}\wp'(t)\right\}. \end{aligned} \tag{19}$$

The Weierstrass function $\wp$ is a doubly periodic elliptic function defined in terms of two parameters g_2 and g_3, called *invariants* – which in our case are real quantities that can be expressed in terms of the initial conditions and of the physical parameters of the system. In case of real invariants, one of the two periods T of $\wp$ and $\wp\prime$ is a purely real quantity. In this respect, we can then consider $\wp$ and $\wp\prime$ as singly periodic functions on the real axis with period T. We refer to Paper I and to classical references such as Abramowitz & Stegun (1964), chapter 18, and Whittaker & Watson (1927) for a more detailed description of the properties of the Weierstrassian functions.

We will now show how it is possible to obtain a simplified form of $H(t)$ which will allow us to proceed to the integration of the angular coordinates.

3 A SIMPLIFIED FORM OF THE SOLUTION FOR *H*

Our starting point is the observation that the coefficient of H^4 in the quartic polynomial $f_4(H)$ in equation (18) is always negative (see eq. (C1) in Paper I). Thus,

$$\lim_{H\to\pm\infty} f_4(H) = -\infty. \tag{20}$$

Additionally, for the radicand in equation (18) to be real (that is, physically meaningful), the polynomial must assume positive values in at least one interval of H. This means that $f_4(H)$ must have two or four real roots (possibly of multiplicity greater than one). Here, we will consider only the cases in which $f_4(H)$ has two or four distinct real roots.[2]

Fig. 1 displays the evolution of $\mathrm{d}H/\mathrm{d}t$ as a function of H in two representative cases.

The existence of real roots for $f_4(H)$ guarantees that we can always express the solution $H(t)$ in a simplified way. By choosing as starting point of the integration of equation (18) one of the roots H_r of $f_4(H)$ (instead of the arbitrary initial value H_0), we have that $f_4(H_\mathrm{r}) = 0$, and thus equation (19) simplifies to

$$H(t) = H_\mathrm{r} + \frac{f_4'(H_\mathrm{r})}{4\left[\wp(t - t_\mathrm{r}) - \frac{1}{24}f_4''(H_\mathrm{r})\right]}, \tag{21}$$

or, for notational convenience,

$$H(t) = H_\mathrm{r} + \frac{A}{\wp(t - t_\mathrm{r}) - B}, \tag{22}$$

where $A = f_4'(H_\mathrm{r})/4$ and $B = f_4''(H_\mathrm{r})/24$ are constants of motion, and t_r is the time at which H assumes the value H_r (where we have chosen as origin of the time coordinate, $t = 0$, the time at which the

[2] Roots with multiplicity greater than one are connected to the existence of equilibrium points, as discussed in section 4.4.2 of Paper I.

system is in the initial conditions). t_r, the time of root passage, can be computed by solving the elliptic integral

$$\int_0^{t_\mathrm{r}} \mathrm{d}t = \pm \int_{H_0}^{H_\mathrm{r}} \frac{\mathrm{d}H}{\sqrt{f_4(H)}}. \tag{23}$$

Here, the $\pm$ sign has to be chosen in accordance with the initial conditions of the system and with the choice of H_r among the roots of $f_4(H)$.

We discuss in detail a concrete example of the computation of t_r in Appendix A.

4 INTEGRATION OF THE ANGULAR COORDINATES

We now turn our attention to the equations of motion for the coordinates g, $h_\star$ and $\tilde{h}$. In general, the equations of motion for the coordinates (equations 32 in Paper I), are built from the partial derivatives of the two components $\mathcal{F}_0$ and $\mathcal{F}_1$ of the Hamiltonian and the cosine of the coordinate $h_\star$, which can also be expressed as a function of $\mathcal{F}_0$ and $\mathcal{F}_1$ after inverting the Hamiltonian (11):

$$\cos h_* = \frac{\mathcal{H}' - \mathcal{H}_N - \varepsilon\mathcal{F}_0}{\varepsilon\mathcal{F}_1}, \tag{24}$$

where, from now on, we will denote with $\mathcal{H}'$ the constant numerical value of the Hamiltonian (obtained by substitution of the initial conditions into equation 11). Equation (24) thus represents the evolution in time of $\cos h_\star$ via its dependence on $H(t)$.

We will now show how all the equations of motion can be expressed as rational functions of the Weierstrass elliptic function $\wp(t)$, and as such they can be integrated with the help of the Weierstrassian functions σ and ζ, and the derivative $\wp'$ and the inverse $\wp^{-1}$ of $\wp$ (the general theory of the integration of rational functions of elliptic functions is outlined in Tannery & Molk (1893) and Greenhill (1959, chapter 7). We will start with the detailed computation of the solution for g; the solutions for the other two coordinates will be formally identical.

The computations that follow are fairly complicated, and they are best tackled with the help of computer algebra. In this paper, we made extensive use of the free computer algebra system SYMPY (SymPy Development Team 2014).

4.1 Solution for the g coordinate

The substitution of the expression for $\cos h_\star$, equation (24), into the equation of motion for $\mathrm{d}g/\mathrm{d}t$,

$$\frac{\mathrm{d}g}{\mathrm{d}t} = \epsilon\left(\frac{\partial\mathcal{F}_0}{\partial G} + \frac{\partial\mathcal{F}_1}{\partial G}\cos h_*\right) \tag{25}$$

(the third one in equations (32) of Paper I), results in a fairly complicated expression. Two crucial simplifications occur:

(i) the square roots in the expression, originating from

$$G_{xy} = \sqrt{G^2 - H^2} \tag{26}$$

and

$$\tilde{G}_{xy*} = \sqrt{\tilde{G}^2 - \left(\tilde{H}_* - H\right)^2}, \tag{27}$$

are either simplified between numerator and denominator, or they are squared. The resulting expression for $\mathrm{d}g/\mathrm{d}t$ will thus be free of square roots and it will be reduced to a rational function of H;

(ii) the resulting rational function can be decomposed in a series of terms which are either linear in H or rational functions of H of degree one in the denominator.

After a full fraction decomposition, the final expression for $\mathrm{d}g/\mathrm{d}t$ as a function of H can be written as

$$\frac{\mathrm{d}g}{\mathrm{d}t} = \Phi_g^0 + \Phi_g^1 H(t) + \frac{1}{G - H(t)}\Phi_g^2 + \frac{1}{G + H(t)}\Phi_g^3 + \frac{1}{G^2 m_2 - H(t) J_2}\Phi_g^4, \tag{28}$$

where Φ_g^i are constants whose full expressions are reproduced in Table 2. Before proceeding, we will first discuss briefly the properties of the right-hand side of equation (28).

4.1.1 *Poles*

The expression on the right-hand side of equation (28) clearly has three potential poles: $H = \pm G$ and $H = G^2 m_2/J_2$. The first two poles, $H = \pm G$, correspond to a singularity in the coordinate system – the angle g is not defined when the orbit is equatorial (which corresponds to the condition $H = \pm G$). This type of singularities is common when working with Delaunay variables (Morbidelli 2002, section 1.9.1).

The third pole, $H = G^2 m_2/J_2$, corresponds to the equilibrium point discussed in section 4.4.1.1 of Paper I, and it derives from the denominator on the right-hand side of equation (24) going to zero. It is easy (although tedious if done by hand) to check that, for $H = G^2 m_2/J_2$, Φ_g^4 also goes to zero, so that the pole is actually an indeterminate form of the type $0/0$.

4.1.2 *On the magnitude of the Φ_g^i constants*

It can be noted by inspecting Table 2 how most, but not all, of the terms composing the Φ_g^i constants are proportional to the small parameter $\varepsilon = 1/c^2$. The absence of the ε multiplicative constant from some of the terms might lead to conclude that the evolution of $\mathrm{d}g/\mathrm{d}t$ in time is 'fast' (e.g. of the same order of magnitude of the mean motion l).

Table 2. Full form of the constants appearing in the expression of $\mathrm{d}g/\mathrm{d}t$, equation (28).

Φ_g^0	$-\frac{5\mathcal{H}'}{G} + \frac{5\mathcal{I}_1\tilde{G}^2}{2G} - \frac{5\mathcal{G}^2 m_2^2}{2GL^2} + \frac{75\mathcal{G}^4\varepsilon m_2^4}{8GL^4} - \frac{21\mathcal{G}^4\varepsilon m_2^4}{2G^2L^3} - \frac{J_2\mathcal{G}^4\tilde{H}_*\varepsilon m_2^3}{2G^4L^3}$
Φ_g^1	$\frac{9J_2\mathcal{G}^4\varepsilon m_2^3}{2G^4L^3}$
Φ_g^2	$\frac{\mathcal{H}'}{2} - \frac{\mathcal{I}_1\tilde{G}^2}{4} + \frac{\mathcal{G}^2 m_2^2}{4L^2} - \frac{15\mathcal{G}^4\varepsilon m_2^4}{16L^4} + \frac{9\mathcal{G}^4\varepsilon m_2^4}{4GL^3} - \frac{3J_2\mathcal{G}^4\varepsilon m_2^3}{2G^2L^3} - \frac{3\mathcal{G}^4\tilde{H}_*\varepsilon m_2^4}{4G^2L^3} + \frac{J_2\mathcal{G}^4\tilde{H}_*\varepsilon m_2^3}{2G^3L^3}$
Φ_g^3	$\frac{\mathcal{H}'}{2} - \frac{\mathcal{I}_1\tilde{G}^2}{4} + \frac{\mathcal{G}^2 m_2^2}{4L^2} - \frac{15\mathcal{G}^4\varepsilon m_2^4}{16L^4} + \frac{9\mathcal{G}^4\varepsilon m_2^4}{4GL^3} + \frac{3J_2\mathcal{G}^4\varepsilon m_2^3}{2G^2L^3} + \frac{3\mathcal{G}^4\tilde{H}_*\varepsilon m_2^4}{4G^2L^3} + \frac{J_2\mathcal{G}^4\tilde{H}_*\varepsilon m_2^3}{2G^3L^3}$
Φ_g^4	$2G\mathcal{H}'m_2 - G\mathcal{I}_1\tilde{G}^2 m_2 + \frac{G\mathcal{G}^2}{L^2}m_2^3 - \frac{15G\mathcal{G}^4\varepsilon}{4L^4}m_2^5 + \frac{3\varepsilon}{L^3}\mathcal{G}^4 m_2^5 - \frac{J_2\mathcal{G}^4\tilde{H}_*\varepsilon}{G^2L^3}m_2^4$

In reality, each fast term is counter-balanced by a corresponding fast term of opposite sign originating from the Hamiltonian constant $\mathcal{H}'$. For instance, if we consider the expression for Φ_g^0,

$$\Phi_g^0 = -\frac{5\mathcal{H}'}{G} + \frac{5\mathcal{I}_1\tilde{G}^2}{2G} - \frac{5\mathcal{G}^2 m_2^2}{2\,G L^2} + \cdots \tag{29}$$

(where we have omitted terms of order ε), and we recall from equation (11) that

$$\mathcal{H}' = \frac{1}{2}\mathcal{I}_1\tilde{G}^2 - \frac{\mathcal{G}^2 m_2^2}{2L^2} + \cdots \tag{30}$$

(where again we have omitted terms of order ε), we can see how the two fast terms in equation (29) (corresponding to the Newtonian part of the Hamiltonian) cancel out with $\mathcal{H}'$ and only terms proportional to ε survive. Similar simplifications occur in all Φ_g^i constants, and thus the evolution of $\mathrm{d}g/\mathrm{d}t$ is slow (i.e. proportional to the small parameter ε).

4.1.3 *Reduction to simpler cases*

Before proceeding to the solution of equation (28), it is interesting to show how $\mathrm{d}g/\mathrm{d}t$ reduces to simpler cases. We have already shown in Paper I how the equation of motion for g reduces to the classical Einstein precession when both spins are absent (section 4.1), and to the Lense–Thirring effect when only the spin of the secondary body is null (section 4.2). Both these results can be checked again by direct substitutions in equation (28).

In section 4.3 of Paper I, we showed how in our formalism the geodetic effect (i.e. the special case in which the central body is not spinning, but the secondary one is) shows up as an equilibrium point corresponding to the initial conditions

$$H = \frac{\tilde{H}_*^2 + G^2 - \tilde{G}^2}{2\tilde{H}_*}, \qquad h_* = \pi + 2k\pi. \tag{31}$$

We also pointed out how this special configuration corresponds to choosing the z-axis aligned to the (constant) total angular momentum of the system, and how it results in the spin and orbital angular momentum vectors precessing around z with the same rate. A result which we did not highlight in Paper I is the effect of the geodetic precession on the g coordinate. After shutting off the J_2 constant and substituting the conditions (31) into equation (28), $\mathrm{d}g/\mathrm{d}t$ simplifies to

$$\frac{\mathrm{d}g}{\mathrm{d}t} = \frac{1}{4G^4L^3}\left(15G^2\mathcal{G}^4\varepsilon m_2^4 + 9\mathcal{G}^4\tilde{G}^2\varepsilon m_2^4 - 9\mathcal{G}^4\tilde{H}_*^2\varepsilon m_2^4\right). \tag{32}$$

That is, the argument of pericentre g precesses with a constant rate which depends on both the orbital angular momentum and the spin state of the secondary body.

4.1.4 *Integration of equation (28)*

We now proceed to the integration by quadrature of equation (28) to determine $g(t)$. Before performing the computation, we can highlight an important property of $g(t)$.

Since $H(t)$ is a periodic function (with a period T that can be computed from the initial conditions of the system, as explained in section 4.4.2 of Paper I), $\mathrm{d}g/\mathrm{d}t$ will also be periodic with the same period T. The integral of a periodic function is an arithmetic quasi-periodic function, that is, $g(t)$ satisfies the relation

$$g(t+T) = g(t) + \Delta_g, \tag{33}$$

Table 3. Terms in $H(t)$ from equation (28) expressed via the $\mathcal{U}(t)$ function, introduced in equation (34).

$H(t)$	$\mathcal{U}(A, B, H_\mathrm{r}; t - t_\mathrm{r})$
$\frac{1}{G-H(t)}$	$\mathcal{U}\left[\frac{A}{(G-H_\mathrm{r})^2}, \frac{A+BG-BH_\mathrm{r}}{G-H_\mathrm{r}}, \frac{1}{G-H_\mathrm{r}}; t-t_\mathrm{r}\right]$
$\frac{1}{G+H(t)}$	$\mathcal{U}\left[-\frac{A}{(G+H_\mathrm{r})^2}, \frac{-A+BG+BH_\mathrm{r}}{G+H_\mathrm{r}}, \frac{1}{G+H_\mathrm{r}}; t-t_\mathrm{r}\right]$
$\frac{1}{G^2m_2-H(t)J_2}$	$\mathcal{U}\left[\frac{AJ_2}{(G^2m_2-H_\mathrm{r}J_2)^2}, \frac{AJ_2+BG^2m_2-BH_\mathrm{r}J_2}{G^2m_2-H_\mathrm{r}J_2}, \frac{1}{G^2m_2-H_\mathrm{r}J_2}; t-t_\mathrm{r}\right]$

where Δ_g is a constant (i.e. independent of t). Thus, the *average* precession rate of $g(t)$ will be Δ_g/T.

The first step for the integration of $\mathrm{d}g/\mathrm{d}t$ is the substitution of the definition of $H(t)$, equation (22), into equation (28). This substitution yields a rational function of $\wp(t - t_\mathrm{r})$. For ease of notation, we can introduce the function

$$\mathcal{U}(\alpha, \beta, \gamma; t) = \frac{\alpha}{\wp(t) - \beta} + \gamma, \tag{34}$$

where it is implied that α, β and γ are constants. With this convention, we can express the terms in $H(t)$ appearing in equation (28) as specific instances of $\mathcal{U}(\alpha, \beta, \gamma; t)$. The correspondence is detailed in Table 3.

The next step is the integration of $\mathcal{U}(\alpha, \beta, \gamma; t)$. The indefinite integral of $\mathcal{U}$ can be expressed via the Weierstrassian elliptic and related functions as (see Tannery & Molk (1893, section CXII) and Gradshteĭn & Ryzhik (2007, equation 5.141.4):

$$\mathcal{V}(\alpha, \beta, \gamma; t) = \int \mathcal{U}(\alpha, \beta, \gamma; t)\,\mathrm{d}t \tag{35}$$

$$= \int \left[\frac{\alpha}{\wp(t) - \beta} + \gamma\right]\mathrm{d}t \tag{36}$$

$$= \frac{\alpha}{\wp'(v)}\left[2t\zeta(v) + \ln\frac{\sigma(t-v)}{\sigma(t+v)}\right] + \gamma t, \tag{37}$$

where $v = \wp^{-1}(\beta)$, and ζ and σ are the Weierstrass zeta and sigma functions (Abramowitz & Stegun 1964, chapter 18).[3] Although $\wp^{-1}$ is a multivalued function, it can be shown that this formula is valid for any choice of v.[4]

We are now ready to write the full expression of $g(t)$ in terms of the $\mathcal{V}$ function introduced in equation (35):

$$g(t) = g_0 + \Phi_g^0 t + \sum_{i=1}^{4}\Phi_g^i\left[\mathcal{V}_g^i(t - t_\mathrm{r}) - \mathcal{V}_g^i(-t_\mathrm{r})\right], \tag{38}$$

where we have introduced a compact notation for the various instances of the $\mathcal{V}$ function appearing in the formula. The full form of the $\mathcal{V}_g^i$ terms is given in Table 4.

Equation (38) represents the final form of the solution for $g(t)$. We now turn our attention to the solution for the other two coordinates.

[3] It must be noted that equation (37) is not valid when $\wp'(v) = 0$ (or, equivalently, when $\wp(v)$ is one of the roots of the characteristic cubic equation associated with $\wp$'s invariants). In such a case, equation (37) must be replaced by the integral formula from Tannery & Molk (1893, section CXII section 2). We will not consider the special case $\wp'(v) = 0$ here.

[4] It should be noted, however, that the multivalued character of the complex logarithm complicates the implementation of equation (37) by introducing discontinuities in correspondence of the branch points. The issue is discussed and addressed in Biscani & Izzo (2014), section A2.

Table 4. Full form of the $\mathcal{V}^i_g(t)$ terms in the solution for $g(t)$, equation (38). The function $\mathcal{V}(t)$ is introduced in equations (35)–(37).

$\mathcal{V}^1_g(t)$	$\mathcal{V}(A, B, H_\mathrm{r}; t)$
$\mathcal{V}^2_g(t)$	$\mathcal{V}\left[\frac{A}{(G-H_\mathrm{r})^2}, \frac{A+BG-BH_\mathrm{r}}{G-H_\mathrm{r}}, \frac{1}{G-H_\mathrm{r}}; t\right]$
$\mathcal{V}^3_g(t)$	$\mathcal{V}\left[-\frac{A}{(G+H_\mathrm{r})^2}, \frac{-A+BG+BH_\mathrm{r}}{G+H_\mathrm{r}}, \frac{1}{G+H_\mathrm{r}}; t\right]$
$\mathcal{V}^4_g(t)$	$\mathcal{V}\left[\frac{AJ_2}{(G^2m_2-H_\mathrm{r}J_2)^2}, \frac{AJ_2+BG^2m_2-BH_\mathrm{r}J_2}{G^2m_2-H_\mathrm{r}J_2}, \frac{1}{G^2m_2-H_\mathrm{r}J_2}; t\right]$

4.2 Solution for the $h\star$ and $\tilde{h}$ coordinates

As hinted earlier, the solution for $h\star(t)$ and $\tilde{h}(t)$ is formally analogous to the solution for $g(t)$. We start by writing the equations of motion for $h\star$ and $\tilde{h}$ after the full fraction decomposition with respect to $H(t)$:

$$\begin{aligned}\frac{\mathrm{d}h_*}{\mathrm{d}t} = {} & \Phi^0_{h_*} + \frac{1}{G - H(t)}\Phi^1_{h_*} + \frac{1}{G + H(t)}\Phi^2_{h_*} \\ & + \frac{1}{G^2m_2 - H(t)J_2}\Phi^3_{h_*} + \frac{1}{H(t) + \tilde{G} - \tilde{H}_*}\Phi^4_{h_*} \\ & + \frac{1}{H(t) - \tilde{G} - \tilde{H}_*}\Phi^5_{h_*},\end{aligned} \tag{39}$$

$$\frac{\mathrm{d}\tilde{h}}{\mathrm{d}t} = \Phi^0_{\tilde{h}} + \frac{1}{H(t) + \tilde{G} - \tilde{H}_*}\Phi^1_{\tilde{h}} + \frac{1}{H(t) - \tilde{G} - \tilde{H}_*}\Phi^2_{\tilde{h}}, \tag{40}$$

where the $\Phi^i_{h_*}$ and $\Phi^i_{\tilde{h}}$ constants are reproduced in full form in Tables 5 and 6. Here, we can note how the expression for $\mathrm{d}h\star/\mathrm{d}t$ is more complicated than the one for $\mathrm{d}\tilde{h}/\mathrm{d}t$, as $h_* = h - \tilde{h}$ contains information on both the orbital angular momentum and the spin of the secondary body.

We can recognize in equations (39) and (40) the singularities discussed in Section 4.1.1, and additional poles for $H = \tilde{H}_* \pm \tilde{G}$. These poles are also arising from a singularity in the coordinate system: for $H = \tilde{H}_* \pm \tilde{G}$ the spin vector of the secondary body is aligned to the z-axis, and the $\tilde{h}$ angle is undefined. We can also verify by substitution that, in the simplified cases of Einstein, Lense–Thirring and geodetic precessions, the formulae for $\mathrm{d}h\star/\mathrm{d}t$ and $\mathrm{d}\tilde{h}/\mathrm{d}t$ collapse to well-known results (see sections 4.1, 4.2 and 4.3 in Paper I).

Table 7. Full form of the $\mathcal{V}^i_{h_*}(t)$ terms in the solution for $h\star(t)$, equation (41).

$\mathcal{V}^1_{h_*}(t)$	$\mathcal{V}\left[\frac{A}{(G-H_\mathrm{r})^2}, \frac{A+BG-BH_\mathrm{r}}{G-H_\mathrm{r}}, \frac{1}{G-H_\mathrm{r}}; t\right]$
$\mathcal{V}^2_{h_*}(t)$	$\mathcal{V}\left[-\frac{A}{(G+H_\mathrm{r})^2}, \frac{-A+BG+BH_\mathrm{r}}{G+H_\mathrm{r}}, \frac{1}{G+H_\mathrm{r}}; t\right]$
$\mathcal{V}^3_{h_*}(t)$	$\mathcal{V}\left[\frac{AJ_2}{(G^2m_2-H_\mathrm{r}J_2)^2}, \frac{AJ_2+BG^2m_2-BH_\mathrm{r}J_2}{G^2m_2-H_\mathrm{r}J_2}, \frac{1}{G^2m_2-H_\mathrm{r}J_2}; t\right]$
$\mathcal{V}^4_{h_*}(t)$	$\mathcal{V}\left[-\frac{A}{(H_\mathrm{r}+\tilde{G}-\tilde{H}_*)^2}, \frac{-A+BH_\mathrm{r}+B\tilde{G}-B\tilde{H}_*}{H_\mathrm{r}+\tilde{G}-\tilde{H}_*}, \frac{1}{H_\mathrm{r}+\tilde{G}-\tilde{H}_*}; t\right]$
$\mathcal{V}^5_{h_*}(t)$	$\mathcal{V}\left[-\frac{A}{(H_\mathrm{r}-\tilde{G}-\tilde{H}_*)^2}, \frac{-A+BH_\mathrm{r}-B\tilde{G}-B\tilde{H}_*}{H_\mathrm{r}-\tilde{G}-\tilde{H}_*}, \frac{1}{H_\mathrm{r}-\tilde{G}-\tilde{H}_*}; t\right]$

Table 8. Full form of the $\mathcal{V}^i_{\tilde{h}}(t)$ terms in the solution for $\tilde{h}(t)$, equation (42).

$\mathcal{V}^1_{\tilde{h}}(t)$	$\mathcal{V}\left[-\frac{A}{(H_\mathrm{r}+\tilde{G}-\tilde{H}_*)^2}, \frac{-A+BH_\mathrm{r}+B\tilde{G}-B\tilde{H}_*}{H_\mathrm{r}+\tilde{G}-\tilde{H}_*}, \frac{1}{H_\mathrm{r}+\tilde{G}-\tilde{H}_*}; t\right]$
$\mathcal{V}^2_{\tilde{h}}(t)$	$\mathcal{V}\left[-\frac{A}{(H_\mathrm{r}-\tilde{G}-\tilde{H}_*)^2}, \frac{-A+BH_\mathrm{r}-B\tilde{G}-B\tilde{H}_*}{H_\mathrm{r}-\tilde{G}-\tilde{H}_*}, \frac{1}{H_\mathrm{r}-\tilde{G}-\tilde{H}_*}; t\right]$

Let us now proceed to the substitution of the expression of $H(t)$ into the equations of motion for $h\star$ and $\tilde{h}$, and to the integration by quadrature via the $\mathcal{V}$ function defined in equation (37). The results are

$$h_*(t) = h_{*,0} + \Phi^0_{h_*}t + \textstyle\sum_{i=1}^5 \Phi^i_{h_*}\left[\mathcal{V}^i_{h_*}(t - t_\mathrm{r}) - \mathcal{V}^i_{h_*}(-t_\mathrm{r})\right], \tag{41}$$

$$\tilde{h}(t) = \tilde{h}_0 + \Phi^0_{\tilde{h}}t + \textstyle\sum_{i=1}^2 \Phi^i_{\tilde{h}}\left[\mathcal{V}^i_{\tilde{h}}(t - t_\mathrm{r}) - \mathcal{V}^i_{\tilde{h}}(-t_\mathrm{r})\right], \tag{42}$$

where the $\mathcal{V}^i_{h_*}$ and $\mathcal{V}^i_{\tilde{h}}$ functions are reproduced in full form in Tables 7 and 8.

Analogously to $g(t)$, both $h\star(t)$ and $\tilde{h}(t)$ are arithmetic quasi-periodic functions of t:

$$h_*(t + T) = h_*(t) + \Delta_{h_*}, \tag{43}$$

$$\tilde{h}(t + T) = \tilde{h}(t) + \Delta_{\tilde{h}}, \tag{44}$$

where T is the period of $H(t)$.

In the case of $h\star(t)$, we can derive an important result about the constant of quasi-periodicity Δ_{h_*}. From equation (24), we know that

Table 5. Full form of the constants appearing in the expression of $\mathrm{d}h\star/\mathrm{d}t$, equation (39).

$\Phi^0_{h_*}$	$-\frac{9J_2\mathcal{G}^4\varepsilon m_2^3}{2G^3L^3} - \frac{3J_2\mathcal{G}^4\tilde{G}^2\varepsilon m_2^3}{2G^5L^3}$
$\Phi^1_{h_*}$	$-\frac{\mathcal{H}'}{2} + \frac{\mathcal{I}_1\tilde{G}^2}{4} - \frac{\mathcal{G}^2m_2^2}{4L^2} + \frac{15\mathcal{G}^4\varepsilon m_2^4}{16L^4} - \frac{9\mathcal{G}^4\varepsilon m_2^4}{4GL^3} + \frac{3J_2\mathcal{G}^4\varepsilon m_2^3}{2G^2L^3} + \frac{3\mathcal{G}^4\tilde{H}_*\varepsilon m_2^4}{4G^2L^3} - \frac{J_2\mathcal{G}^4\tilde{H}_*\varepsilon m_2^3}{2G^3L^3}$
$\Phi^2_{h_*}$	$\frac{\mathcal{H}'}{2} - \frac{\mathcal{I}_1\tilde{G}^2}{4} + \frac{\mathcal{G}^2m_2^2}{4L^2} - \frac{15\mathcal{G}^4\varepsilon m_2^4}{16L^4} + \frac{9\mathcal{G}^4\varepsilon m_2^4}{4GL^3} + \frac{3J_2\mathcal{G}^4\varepsilon m_2^3}{2G^2L^3} + \frac{3\mathcal{G}^4\tilde{H}_*\varepsilon m_2^4}{4G^2L^3} + \frac{J_2\mathcal{G}^4\tilde{H}_*\varepsilon m_2^3}{2G^3L^3}$
$\Phi^3_{h_*}$	$-J_2\mathcal{H}' + \frac{J_2\mathcal{I}_1}{2}\tilde{G}^2 - \frac{J_2\mathcal{G}^2m_2^2}{2L^2} + \frac{15J_2\mathcal{G}^4\varepsilon}{8L^4}m_2^4 - \frac{3J_2\mathcal{G}^4\varepsilon m_2^4}{2GL^3} + \frac{J_2^2\mathcal{G}^4\tilde{H}_*\varepsilon m_2^3}{2G^3L^3}$
$\Phi^4_{h_*}$	$\frac{\mathcal{H}'}{2} - \frac{\mathcal{I}_1\tilde{G}^2}{4} + \frac{\mathcal{G}^2m_2^2}{4L^2} - \frac{15\mathcal{G}^4\varepsilon m_2^4}{16L^4} + \frac{3\mathcal{G}^4\varepsilon m_2^4}{2GL^3} + \frac{3J_2\mathcal{G}^4\tilde{G}\varepsilon m_2^3}{4G^3L^3} - \frac{J_2\mathcal{G}^4\tilde{H}_*\varepsilon}{G^3L^3}m_2^3 + \frac{3\mathcal{G}^4\tilde{G}^2\varepsilon m_2^4}{4G^3L^3} - \frac{3\mathcal{G}^4\tilde{G}\tilde{H}_*\varepsilon m_2^4}{4G^3L^3} + \frac{3J_2\mathcal{G}^4\tilde{G}^3\varepsilon m_2^3}{4G^5L^3} - \frac{3J_2\mathcal{G}^4\tilde{G}^2\tilde{H}_*\varepsilon}{2G^5L^3}m_2^3 + \frac{3J_2\mathcal{G}^4\tilde{G}\tilde{H}_*^2\varepsilon}{4G^5L^3}m_2^3$
$\Phi^5_{h_*}$	$\frac{\mathcal{H}'}{2} - \frac{\mathcal{I}_1\tilde{G}^2}{4} + \frac{\mathcal{G}^2m_2^2}{4L^2} - \frac{15\mathcal{G}^4\varepsilon m_2^4}{16L^4} + \frac{3\mathcal{G}^4\varepsilon m_2^4}{2GL^3} - \frac{3J_2\mathcal{G}^4\tilde{G}\varepsilon m_2^3}{4G^3L^3} - \frac{J_2\mathcal{G}^4\tilde{H}_*\varepsilon}{G^3L^3}m_2^3 + \frac{3\mathcal{G}^4\tilde{G}^2\varepsilon m_2^4}{4G^3L^3} + \frac{3\mathcal{G}^4\tilde{G}\tilde{H}_*\varepsilon m_2^4}{4G^3L^3} - \frac{3J_2\mathcal{G}^4\tilde{G}^3\varepsilon m_2^3}{4G^5L^3} - \frac{3J_2\mathcal{G}^4\tilde{G}^2\tilde{H}_*\varepsilon}{2G^5L^3}m_2^3 - \frac{3J_2\mathcal{G}^4\tilde{G}\tilde{H}_*^2\varepsilon}{4G^5L^3}m_2^3$

Table 6. Full form of the constants appearing in the expression of $\mathrm{d}\tilde{h}/\mathrm{d}t$, equation (40).

$\Phi^0_{\tilde{h}}$	$\frac{2J_2\mathcal{G}^4\varepsilon}{G^3L^3}m_2^3 + \frac{3J_2\mathcal{G}^4\tilde{G}^2\varepsilon m_2^3}{2G^5L^3}$
$\Phi^1_{\tilde{h}}$	$-\frac{\mathcal{H}'}{2} + \frac{\mathcal{I}_1\tilde{G}^2}{4} - \frac{\mathcal{G}^2m_2^2}{4L^2} + \frac{15\mathcal{G}^4\varepsilon m_2^4}{16L^4} - \frac{3\mathcal{G}^4\varepsilon m_2^4}{2GL^3} - \frac{3J_2\mathcal{G}^4\tilde{G}\varepsilon m_2^3}{4G^3L^3} + \frac{J_2\mathcal{G}^4\tilde{H}_*\varepsilon}{G^3L^3}m_2^3 - \frac{3\mathcal{G}^4\tilde{G}^2\varepsilon m_2^4}{4G^3L^3} + \frac{3\mathcal{G}^4\tilde{G}\tilde{H}_*\varepsilon m_2^4}{4G^3L^3} - \frac{3J_2\mathcal{G}^4\tilde{G}^3\varepsilon m_2^3}{4G^5L^3} + \frac{3J_2\mathcal{G}^4\tilde{G}^2\tilde{H}_*\varepsilon}{2G^5L^3}m_2^3 - \frac{3J_2\mathcal{G}^4\tilde{G}\tilde{H}_*^2\varepsilon}{4G^5L^3}m_2^3$
$\Phi^2_{\tilde{h}}$	$-\frac{\mathcal{H}'}{2} + \frac{\mathcal{I}_1\tilde{G}^2}{4} - \frac{\mathcal{G}^2m_2^2}{4L^2} + \frac{15\mathcal{G}^4\varepsilon m_2^4}{16L^4} - \frac{3\mathcal{G}^4\varepsilon m_2^4}{2GL^3} + \frac{3J_2\mathcal{G}^4\tilde{G}\varepsilon m_2^3}{4G^3L^3} + \frac{J_2\mathcal{G}^4\tilde{H}_*\varepsilon}{G^3L^3}m_2^3 - \frac{3\mathcal{G}^4\tilde{G}^2\varepsilon m_2^4}{4G^3L^3} - \frac{3\mathcal{G}^4\tilde{G}\tilde{H}_*\varepsilon m_2^4}{4G^3L^3} + \frac{3J_2\mathcal{G}^4\tilde{G}^3\varepsilon m_2^3}{4G^5L^3} + \frac{3J_2\mathcal{G}^4\tilde{G}^2\tilde{H}_*\varepsilon}{2G^5L^3}m_2^3 + \frac{3J_2\mathcal{G}^4\tilde{G}\tilde{H}_*^2\varepsilon}{4G^5L^3}m_2^3$

$\cos[h_*(t)]$ is a periodic function of t with period T. Consequently,

$$\cos[h_*(t)] = \cos[h_*(t+T)] \tag{45}$$

$$= \cos[h_*(t)]\cos\Delta_{h_*} - \sin[h_*(t)]\sin\Delta_{h_*}. \tag{46}$$

Thus $\Delta_{h_*} = 2k\pi$ with $k \in \mathbb{Z}$. The geometrical meaning of this result is that the angular distance between the two nodal angles h and $\tilde{h}$ is, on average, constant modulo $2k\pi$.

5 APPLICATION TO PHYSICAL SYSTEMS

We proceed now to the application of the results outlined in the previous sections to physical systems of interest. We must emphasize how, in light of our initial assumptions, the systems considered here are highly idealized. Indeed, our objective is not to produce accurate descriptions of realistic physical models, but rather to highlight the role that purely relativistic effects play in the dynamical evolution of these systems, and to emphasize the novelties introduced by our solution with respect to the classical results.

We will see that the various relativistic effects have different sensitivities to the physical parameters and to the initial conditions of the system. In particular, the interaction between the spin and the orbital angular momentum of the secondary body is driven by the relative magnitude of the two quantities. Similarly, the timescales over which the effects manifest themselves (and in particular the period T of $H(t)$) are also wildly different in the examples considered.

In order to avoid complications arising from the limited precision of floating-point arithmetic on contemporary machines, the computations presented in the following sections were all performed with the multiprecision PYTHON floating-point arithmetic library MPMATH (Johansson et al. 2014).

5.1 Pulsar planet

As a first example, we revisit the case of a planet in close orbit around a pulsar, which was the subject of an initial analysis in Paper I. Pulsar planets are detected by precise measurements of anomalies in the pulsation period of the host star. Although rarer than other types of exoplanets, a number of pulsar planets have already been discovered and studied (Wolszczan & Frail 1992; Ford et al. 2000; Bailes et al. 2011).

In this specific case, we will study the dynamics of a pulsar planet similar to PSR J1719-1438b (Bailes et al. 2011). The PSR J1719-1438 system is composed of a millisecond pulsar and a smaller planet-size object in close orbit around it. This object is a former white dwarf companion to the main star that lost most of its matter and was consequently reclassified as a planet. The planet is roughly similar to Jupiter in mass, and its orbit around the pulsar has a semimajor axis smaller than a solar radius. The physical parameters and the initial conditions of our model are displayed in Table 9.

Before proceeding, we must emphasize the limitations of our model in this specific scenario:

(i) the magnitude of the spin of the pulsar is not much larger than the magnitude of the orbital spin, and thus we are in a limit case with respect to the assumption that the spin of the pulsar is fixed;

(ii) the planet's estimated density is similar to the density of Jupiter, and thus we can expect that Newtonian figure effects will play a considerable role in the real dynamics. Additionally, in presence of sufficiently extended bodies the *effacement theorem* that allows us to treat the bodies as point particles may cease to be a valid approximation (Damour 1987).

Table 9. Physical parameters and initial conditions of the pulsar planetary system analysed in Section 5.1, inspired by the PSR J1719-1438 system described in Bailes et al. (2011).

Star mass	$1.4\,M_\odot$
Star rotation period	5 ms
Star radius	20 km
Planetary rotation period	9.9 h
Planetary radius	35 000 km
Planetary spin inclination	28°.6
Longitude of the node of the planetary spin ($\tilde{h}$)	0°
Argument of pericentre (g)	0°
Orbital semimajor axis	600 000 km
Orbital eccentricity	0.1
Orbital inclination	45°.8
Longitude of the orbital node (h)	114°.6

5.1.1 *Modifications to the standard precession motions*

The first step of our analysis is the quantification of the effects of the spins on the standard precession motions. The precession of the pericentre in absence of spin (i.e. the Einstein precession) for this system can be calculated using standard formulae (Einstein 1916; Straumann 1984), and it amounts to $17°.498\ \mathrm{yr}^{-1}$. If only the spin of the central body is taken into account, the precession of the pericentre is modified to $17°.484\ \mathrm{yr}^{-1}$ (Bogorodskii 1959; Cugusi & Proverbio 1978). In both cases, the precessions are linear – that is, $g(t)$ is a linear function of the time t.

If we consider the rotation of both the central star and of the orbiting planet, then $g(t)$ is given by equation (38). As explained earlier, in our solution $g(t)$ is a quasi-periodic function expressed in terms of the Weierstrassian functions. The average precession rate can then be computed as

$$\omega_g = \frac{g(T) - g(0)}{T}, \tag{47}$$

where T is the period of $H(t)$ (and the quasi-period of $g(t)$), which, for this particular system, amounts to 41.177 yr. The numerical value of ω_g is $17°.481\ \mathrm{yr}^{-1}$. This means that, on average, in this specific system the full interaction between the spins and the orbit alters the classical precession rates by a relative amount of roughly 10^{-4} (corresponding to a linear displacement of the pericentre of a few tens of kilometres per year with respect to the classical results[5]).

Additionally, the full spin–orbit interaction overlays a periodic modulation on to the average precession rate. The period of this modulation is again $T = 41.177$ yr, and its amplitude is circa 0°.025. The plots in Fig. 2 provide a graphical visualization of the various relativistic effects on the argument of pericentre.

A similar analysis can be undertaken for the longitude of the ascending orbital node h. In absence of spins, the orbital plane is fixed in space and h is thus constant. If only the spin of the central body is taken into account, the orbital plane starts rotating around the spin's axis with a constant rate and $h(t)$ becomes a linear function of the time t. This effect is sometimes referred to as Lense–Thirring precession (Thirring 1918), and, in this specific

[5] For comparison, the decay of the orbital radius induced by the emission of gravitational waves in the binary pulsar PSR J0737-3039 amounts to 2.6 m yr^{-1} (Lyne et al. 2004).

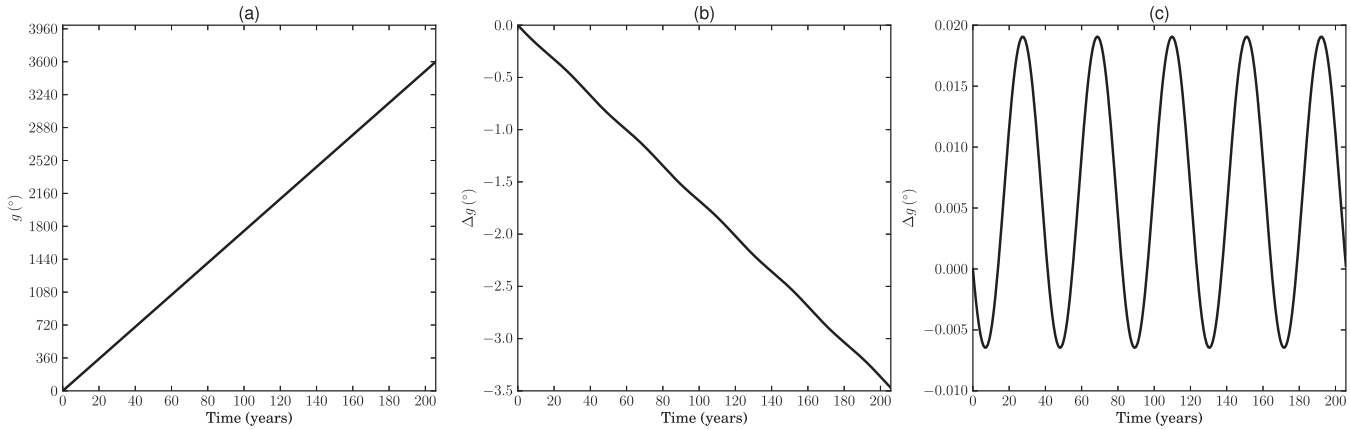

Figure 2. Evolution in time of the argument of pericentre g in the pulsar planetary system presented in Section 5.1. Panel (a) visualizes the standard Einstein precession (i.e. the simplified case in which both spins are turned off). In this case, g is a linear function of time. Panel (b) plots the difference between the Einstein precession and the quasi-periodic precession described by equation (38), where both spins are fully taken into account. Panel (c) displays the difference between equation (38) and its average counterpart, highlighting the periodic modulation superimposed over the average precession rate (barely visible also in panel b).

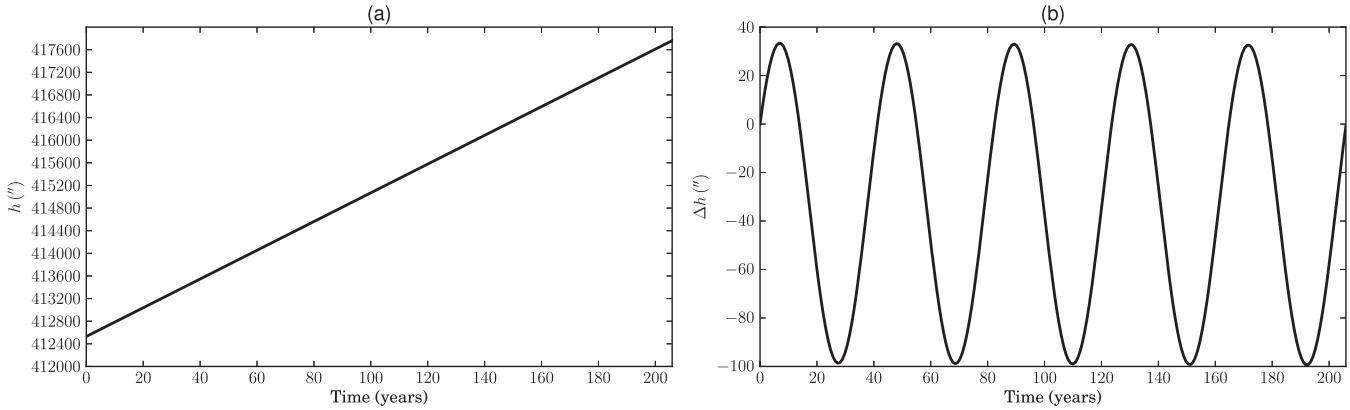

Figure 3. Evolution in time of the longitude of the ascending orbital node h in the pulsar planetary system presented in Section 5.1. Panel (a) visualizes the standard Lense–Thirring precession (i.e. the simplified case in which only the central body is spinning). In this case, h is a linear function of time. Panel (b) plots the difference between the Lense–Thirring precession and the full quasi-periodic solution for $h(t)$ (which can be computed via the sum of equations 41 and 42), where both spins are fully taken into account. It can be recognized how, in panel (b), the local minima of the periodic modulation move progressively to the bottom, due to the quasi-periodic character of the motion.

example, it amounts to 25.403 arcsec yr^{-1}. In a similar fashion to g, the full spin–orbit interaction modifies the average precession rate of h to 25.399 arcsec yr^{-1}, and thus the relative difference with the classical precession rate is again of the order of 10^{-4}. The periodic modulation of h has an amplitude of circa 0.°036. Fig. 3 provides a graphical visualization of the relativistic effects on the longitude of the ascending orbital node.

We turn now our attention to the study of the evolution of the spin of the planet. If the spin of the central star is turned off, then both the orbital angular momentum and the spin of the planet rotate around the (constant) total angular momentum vector with a constant angular velocity. This classical result is often referred to as de Sitter precession (de Sitter 1916; Schiff 1960a,b). Cast into SA variables, the de Sitter precession results in an evolution of the angle $\tilde{h}$ which is either periodic or quasi-periodic, depending on the geometry of the system.[6]

In our specific model, the de Sitter effect shows up as a quasi-periodic evolution of the angle $\tilde{h}$, with an average rate of 8.°7502 yr^{-1}.[7] This rate is modified to 8.°7499 yr^{-1} once the full solution from equation (42) is taken into account. Besides, the complete spin–orbit interaction results in an additional quasi-periodic modulation of the $\tilde{h}$ angle, which, over the course of 200 yr, reaches a maximum amplitude of roughly 3.°5. The geometric interpretation of this result is that the full solution introduces an additional drifting of the planetary spin with respect to the standard de Sitter precession, driven by the spin–spin interaction. The situation is visualized graphically in the plots of Fig. 4.

We conclude this section with the inclusion of a plot of the three-dimensional evolution in time of the orbital angular momentum

[6] This duality of character is merely an artefact of the coordinate system. From a geometrical point of view, the de Sitter effect is always a precession around the total angular momentum. If the precession cone encompasses the z-axis, then the precession shows up as a quasi-periodic evolution of $\tilde{h}$ with a constant of quasi-periodicity of 2π. Otherwise, the evolution in time of $\tilde{h}$ is periodic.

[7] It can be noted how, in the case of de Sitter effect, the period T of $H(t)$ coincides exactly with the period of the precession, as shown in section 5.4 of Paper I.

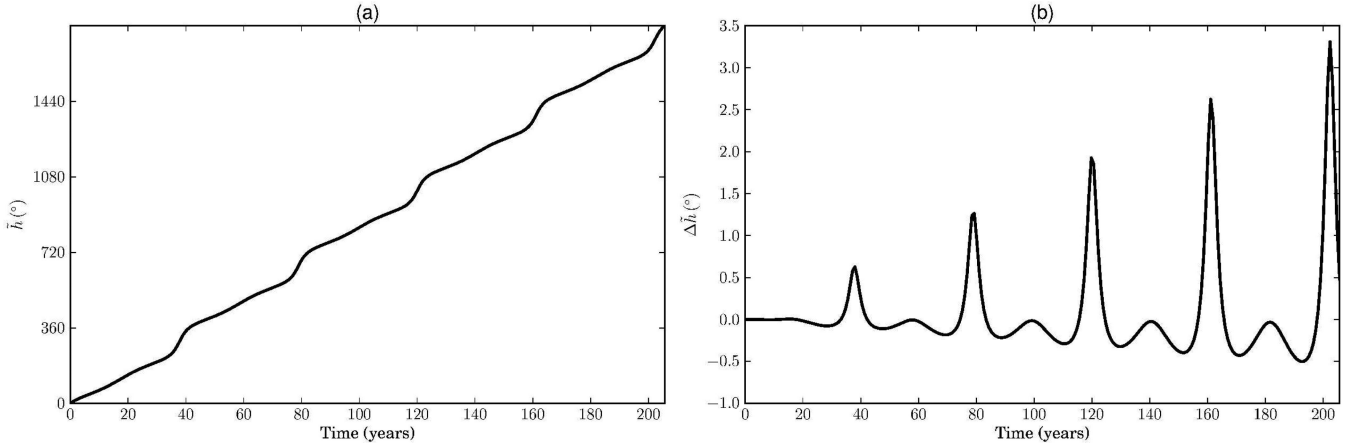

Figure 4. Evolution in time of the longitude of the ascending node of the planetary spin $\tilde{h}$ in the pulsar planetary system presented in Section 5.1. Panel (a) visualizes the standard de Sitter precession (i.e. the simplified case in which only the planetary body is spinning). In this case, $\tilde{h}$ is a quasi-periodic function of time originating from the projection of the precession motion of the spin on to the invariant plane of the inertial reference system. Panel (b) plots the difference between the de Sitter precession and the full solution for $\tilde{h}\,(t)$ (equation 42), where both spins are taken into account.

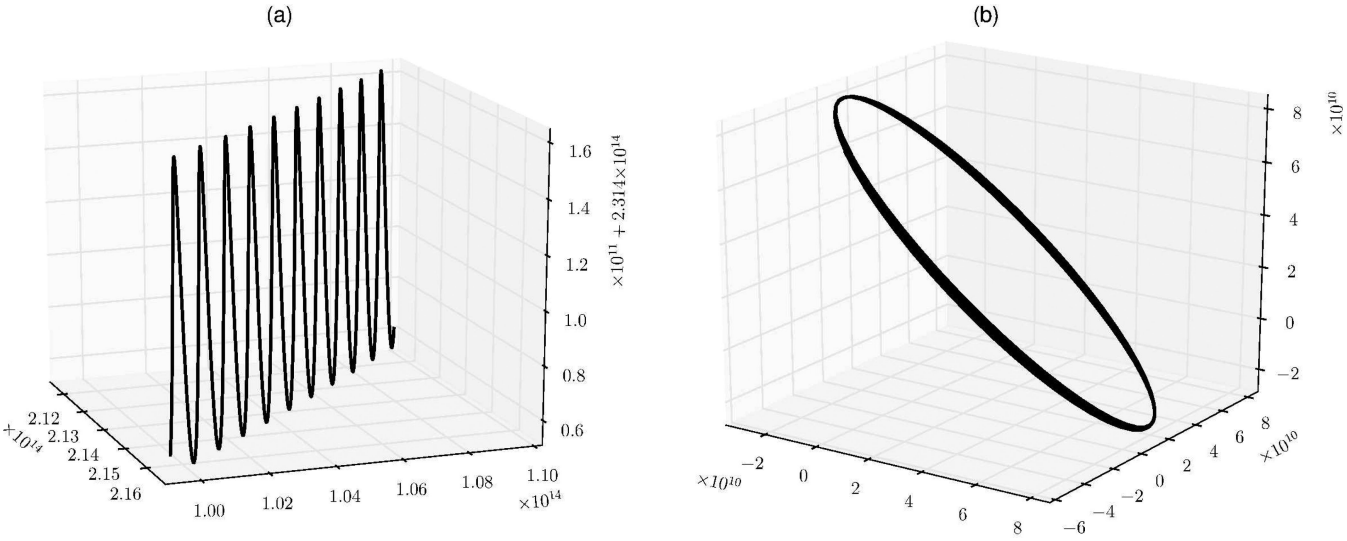

Figure 5. Three-dimensional plots of the evolution in time of the orbital angular momentum (panel a) and of the spin vector (panel b) of the secondary body in the pulsar planetary system presented in Section 5.1. Both quantities are normalized by the mass of the secondary body and represented in SI units. The evolution is followed for 10 periods of $H(t)$, corresponding to circa 410 yr. The orbital angular momentum is subject to a secular drift modulated by a periodic motion, while the spin vector draws a precession figure that slowly rotates in time. It can be noted how the precession cone includes the z-axis and thus the evolution of the nodal angle (plotted in Fig. 4) is quasi-periodic (rather than purely periodic).

and of the spin vector of the planet, visualized in Fig. 5. The plot displays the evolution of the two vectors, when the full interaction between spins and orbit is taken into account.

5.1.2 *Relativistic nutation in obliquity*

In addition to the semiperiodic modifications to the standard relativistic precession rates presented in the previous section, our solution highlights an effect on the obliquity of the secondary body. We recall that the orbital angular momentum vector (normalized by the planet's mass) is given by

$$\left(\sqrt{G^2-H^2}\cos h, -\sqrt{G^2-H^2}\sin h, H\right), \tag{48}$$

in Delaunay variables and, similarly, the normalized spin vector is given by

$$\left(\sqrt{\tilde{G}^2-\tilde{H}^2}\cos\tilde{h}, -\sqrt{\tilde{G}^2-\tilde{H}^2}\sin\tilde{h}, \tilde{H}\right) \tag{49}$$

in SA variables. We can then easily compute the cosine of the angular separation θ between the two vectors via their dot product as

$$\cos\theta = \frac{\sqrt{G^2-H^2}\sqrt{\tilde{G}^2-\left(\tilde{H}_*-H\right)^2}\cos h_* + H\left(\tilde{H}_*-H\right)}{G\tilde{G}}. \tag{50}$$

We can then note how, since both $H(t)$ and $\cos[h_*(t)]$ are periodic functions with period T, then $\cos[\theta(t)]$ is also periodic with the same period T. Fig. 6 displays the evolution in time of the obliquity of the planet. The amplitude of the oscillatory motion amounts, in

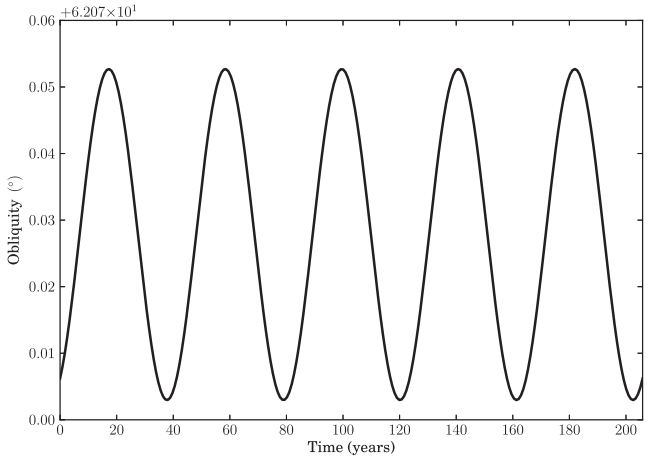

Figure 6. Evolution in time of the obliquity of the secondary body in the pulsar planetary system presented in Section 5.1.

Table 10. Physical parameters and initial conditions of the SMBH-pulsar system analysed in Section 5.2, inspired by the S2 star orbiting Sgr A* (Sabha et al. 2012).

SMBH mass	$4.3 \times 10^6\ M_\odot$
SMBH spin parameter	0.99
Pulsar rotation period	5 ms
Pulsar radius	20 km
Pulsar spin inclination	28.°6
Longitude of the node of the pulsar spin ($\tilde{h}$)	0°
Argument of pericentre (g)	0°
Orbital semimajor axis	600 au
Orbital eccentricity	0.8
Orbital inclination	45.°8
Longitude of the orbital node (h)	114.°6

this case, to circa 0.°05. As far as we have been able to verify in the literature, this is the first time that this purely relativistic nutation in obliquity is reported.

5.2 Pulsar orbiting an SMBH

In this second example, we shall examine the dynamics of a pulsar orbiting a supermassive black hole (SMBH). Stars in close orbit around the SMBH at the centre of the Milky Way, Sgr A*, have been recently discovered and studied (Meyer et al. 2012; Sabha et al. 2012), and, with the availability of next-generation instruments for astrometry, they have become prime candidates for accurate tests of the theory of General Relativity (Eisenhauer et al. 2011). Pulsars, in particular, have the potential to provide novel tests of General Relativity via accurate timing measurements (Liu et al. 2012).

In our model, the SMBH has a mass of 4.3 million solar masses, and a spin parameter of 0.99.[8] The orbiting pulsar is assumed to have a diameter of 20 km and a period of 5 ms. The initial conditions of its orbit are inspired by those of the S2 star (Sabha et al. 2012): the semimajor axis is 600 au and the eccentricity is 0.8. The orientation of the orbit in space has been chosen equal to that of the pulsar planet described in 5.1. Table 10 displays the details of the setup of our model. Although the relativistic effects are very strong in this gravitational regime, the orbit of the star is still quasi-Keplerian (as determined by direct observations), and we can expect low-order PN expansions to remain a good approximation of the real motion on sufficiently small time-scales.

We need again to point out the limitations of our model in this scenario:

(i) the galactic centre is a rich environment, and thus the orbit of the star around the SMBH is likely to be influenced substantially by the presence of other masses;
(ii) we ignore the spin-quadratic contributions due to monopole–quadrupole interaction (which for black holes are given, e.g. in Damour 2001).

Our analysis starts with the quantification of the relativistic effects on the orbit of the pulsar. The Einstein precession for this system amounts to $0.°029\,72\ \mathrm{yr}^{-1}$. The inclusion of the spin of the SMBH alters this value to $0.°029\,28\ \mathrm{yr}^{-1}$. The additional inclusion of the spin of the pulsar in the model has a small effect: the average precession rate is modified by a relative amount of circa 7×10^{-10}. The period of $H(t)$ for this system is 24 600 yr, and the oscillation of g with respect to the average precession rate has an amplitude of circa 0.5 mas.

Regarding the Lense–Thirring effect, in this system the classical precession of the orbital node amounts to $0.°021\,44\ \mathrm{century}^{-1}$. When we take into account the full solution for $h(t)$, the average precession rate is modified by a relative amount of circa 10^{-9}, whereas the periodic oscillations overlaid on the average precession motion have an amplitude of circa 0.7 mas. The evolution of h in time is visualized in Fig. 7.

Moving now to the analysis of the evolution of the spin of the pulsar, the de Sitter effect for this system shows up as a precession of the nodal angle of the spin $\tilde{h}$ with an average rate of circa $0.°014\,86\ \mathrm{yr}^{-1}$. The inclusion of the central spin in the model modifies this rate to $0.°014\,85\ \mathrm{yr}^{-1}$, and overlays additional quasi-periodic variations whose amplitude increases in time (see Fig. 8). The relativistic nutation in obliquity for this system amounts to circa 0.°8, as visualized in Fig. 9. Lastly, we include a plot visualizing the three-dimensional evolution of the orbital angular momentum and spin vectors of the pulsar in Fig. 10.

It is clear from our analysis that this system behaves differently from the pulsar planetary system described in the previous section. The effect of the full solution on the orbit of the secondary body is less pronounced in the SMBH-pulsar system (amounting to modifications of the order of 10^{-10}–10^{-9} with respect to the classical precession rates). On the other hand, the spin of the SMBH interacts strongly with the spin of the orbiting star, and the effects of the full solution are more evident on the evolution of the spin of the pulsar. In particular, the amplitude of the nutation in obliquity of the secondary body is one order of magnitude greater than in the pulsar planetary system.

5.3 Jupiter-orbiting satellites

In the next example, we will examine the relativistic dynamics of two spinning natural satellites in orbit around a Jupiter-like planet. The first satellite is an Io-like object, whereas the second satellite is an inner and smaller moon modelled after Metis. As usual, all the bodies are assumed to be homogeneous spheres and the reference plane is chosen perpendicular to the planet's rotation axis. The two satellites are considered separately and thus assumed not to interact with each other.

[8] Although it is established that Sgr A* is a spinning black hole, its spin parameter is not well determined yet. Values from 0.2 to 0.99 have been reported in the literature (Genzel et al. 2003; Aschenbach 2005; Kato et al. 2010; Liu et al. 2012).

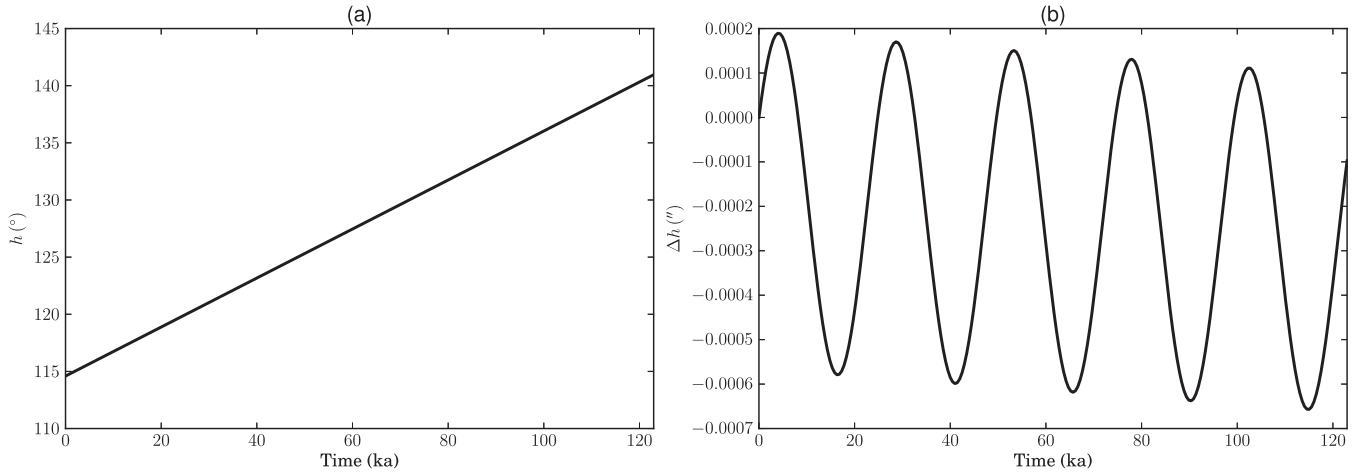

Figure 7. Evolution in time of the longitude of the ascending orbital node h in the SMBH-pulsar system presented in Section 5.2. Panel (a) visualizes the standard Lense–Thirring precession (i.e. the simplified case in which only the central body is spinning). Panel (b) plots the difference between the Lense–Thirring precession and the full quasi-periodic solution for $h(t)$, where both spins are fully taken into account.

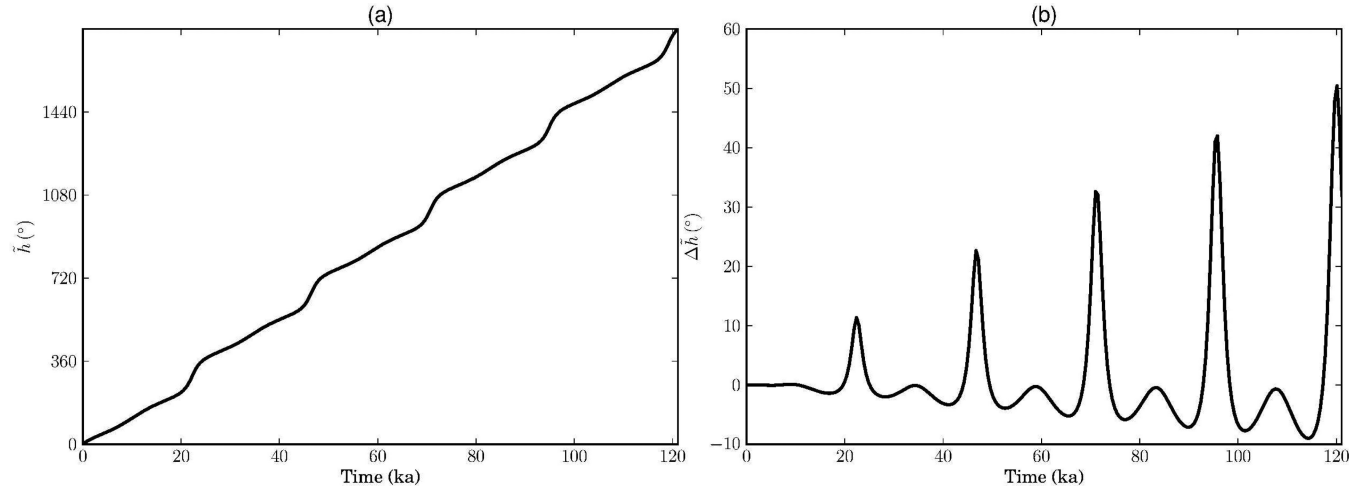

Figure 8. Evolution in time of the longitude of the ascending node of the spin of the pulsar $\tilde{h}$ in the SMBH-pulsar system presented in Section 5.2. Panel (a) visualizes the standard de Sitter precession (i.e. the simplified case in which only the planetary body is spinning). Panel (b) plots the difference between the de Sitter precession and the full solution for $\tilde{h}\,(t)$, where both spins are taken into account.

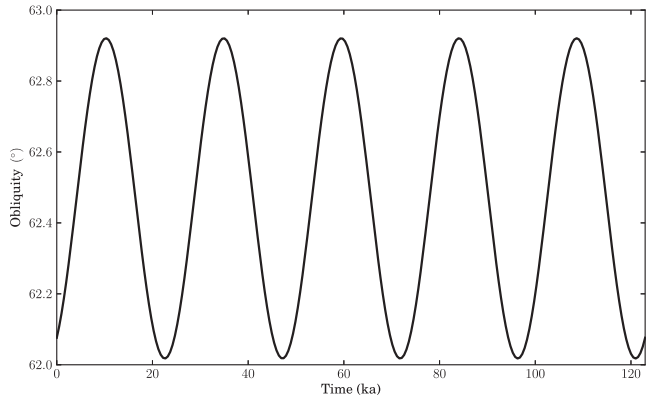

Figure 9. Evolution in time of the obliquity of the secondary body in the SMBH-pulsar system presented in Section 5.2.

We will setup the dynamical system in two different ways. In the first setup, we will choose a set of initial conditions similar to those of the present-day Io and Metis. In particular, the two bodies are tidally locked with the primary, they are moving on almost-circular and almost-equatorial orbits, and their obliquities are almost zero.[9] In the second setup, we will increase the rotation speed, eccentricity, inclination, and obliquity of both bodies. The details of both setups are presented in Table 11.

This system is an interesting subject of study because of Jupiter's mass and fast rotation, because of the close orbits of the two satellites and because the system is accessible to direct observations. Additionally, the second setup could yield useful results concerning the dynamical evolution of the satellites before they settled in the

[9] The obliquity of the Galilean satellites is not yet observed, but it is assumed to be small (Bills 2005; Baland, Yseboodt & Hoolst 2012). The obliquity of the inner moons of Jupiter is also assumed to be small (Thomas et al. 1998).

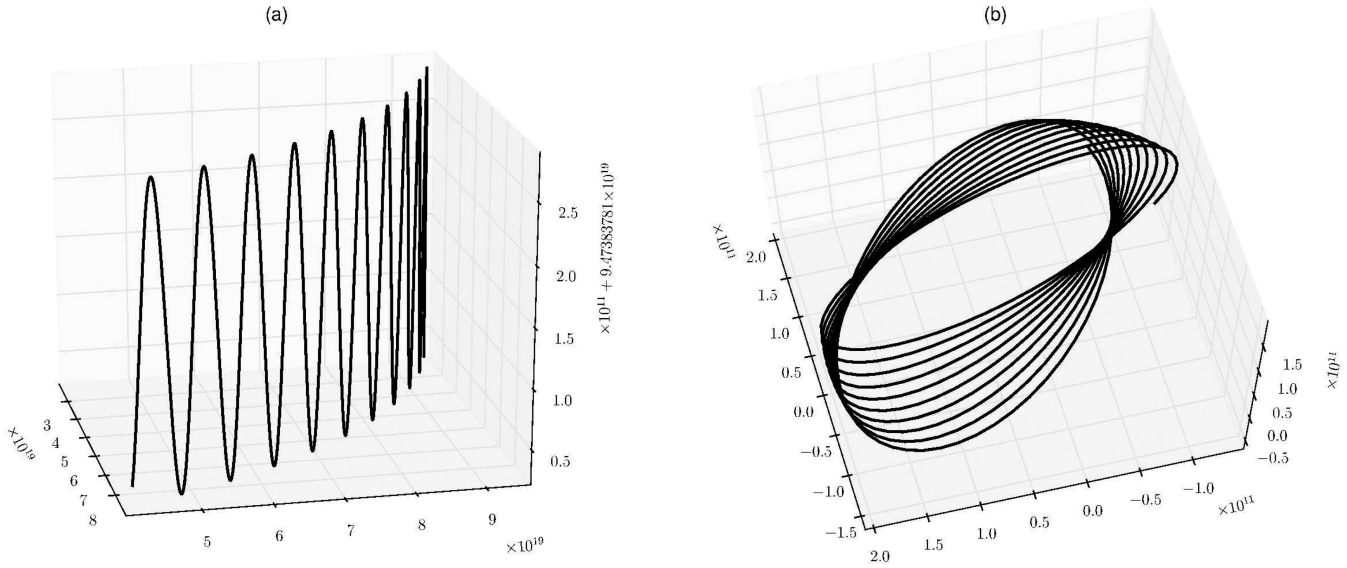

Figure 10. Three-dimensional plots of the evolution in time of the orbital angular momentum (panel a) and of the spin vector (panel b) of the secondary body in the SMBH-pulsar system presented in Section 5.2. Both quantities are normalized by the mass of the secondary body and represented in SI units. The evolution is followed for 10 periods of $H(t)$, corresponding to circa 250 000 yr.

Table 11. Physical parameters and initial conditions of the dynamical system analysed in Section 5.3, consisting of a Jupiter-sized central planet orbited by two natural satellites, one similar to Io and the other similar to Metis.

	Setup 1	Setup 2
Planet mass	1.9×10^{27} kg	
Planet rotation period	9.925 h	
Planet radius	70 000 km	
Rotation period (Io)	42 h	21 h
Radius (Io)	1821 km	
Obliquity (Io)	1°	10°
Longitude of the spin node (Io)	0°	
Argument of pericentre (Io)	0°	
Eccentricity (Io)	0.0041	0.05
Semimajor axis (Io)	421 700 km	
Inclination (Io)	0.°5	20°
Longitude of the orbital node (Io)	20°	
Rotation period (Metis)	7 h	3.5 h
Radius (Metis)	20 km	
Obliquity (Metis)	1°	10°
Longitude of the spin node (Metis)	0°	
Argument of pericentre (Metis)	0°	
Eccentricity (Metis)	0.0002	0.05
Semimajor axis (Metis)	128 000 km	
Inclination (Metis)	0.°5	20°
Longitude of the orbital node (Metis)	20°	

almost-equilibrium position that they occupy today (see Murray & Dermott 2000, chapters 4 and 5). The main limitations of our model in this scenario are that the real satellites are not perfectly spherical (especially Metis), and that the complex dynamical environment around Jupiter is not taken into account.

5.3.1 *Setup 1*

For the Io-like object, the Einstein precession in the first setup amounts to 0.°0746 century^{-1} without Jupiter's spin, and to 0.°0675 century^{-1} with Jupiter's spin. The Lense–Thirring precession amounts to 0.°002 34 century^{-1}. The full solution modifies the average precession of the pericentre by a relative amount of circa 7.5×10^{-6} and the average Lense–Thirring effect by a relative amount of 1.2×10^{-5}. The period of $H(t)$ is 1.066 Ma, and the periodic oscillation of the argument of pericentre with respect to the average precession reaches an amplitude of about 0.°001. Finally, the nutation in obliquity has an amplitude of circa 0.°05.

For the Metis-like object, the classical Einstein precession amounts to 1.°469 century^{-1}, modified to 1.°218 century^{-1} by the inclusion of the rotation of Jupiter in the model. The Lense–Thirring precession amounts to 0.°0838 century^{-1}. The full solution alters the values of the average pericentre and Lense–Thirring precessions by a relative amount of circa 10^{-8}. The period of $H(t)$ is 59.13 ka and the nutation in obliquity has an amplitude of about 0.°1.

As discussed in Paper I, in this setup the two satellites are very close to an equilibrium point, and thus the dynamical quantities are subject to small variations in time.

5.3.2 *Setup 2*

In the second setup, the Einstein precession for the Io-like object amounts to 0.°0747 century^{-1} without Jupiter's spin and to 0.°0681 century^{-1} with Jupiter's spin. The Lense–Thirring precession of the orbital node amounts to 0.°002 35 century^{-1}. The full solution modifies the average precession rates by relative amounts of 1.5×10^{-5} (Einstein) and 2.3×10^{-5} (Lense–Thirring). The period of $H(t)$ is 1.057 Ma, and the nutation in obliquity has an amplitude of circa 2°.

For the Metis-like object, the classical Einstein precession amounts to 1.°473 century^{-1}, modified to 1.°236 century^{-1} by the inclusion of the rotation of Jupiter in the model. The Lense–Thirring precession amounts to 0.°0841 century^{-1}. The period of $H(t)$ is 58.24 ka and the nutation in obliquity has an amplitude of almost 4°.

It is clear that the geometric differences of this setup with respect to the first one introduce appreciable variations in the dynamics. The standard precession rates are modified slightly by the changes

Table 12. Physical parameters and initial conditions of the dynamical system analysed in Section 5.4, consisting of the Earth–Moon system orbiting the Sun.

Star mass	$1\,M_\odot$
Star radius	695 500 km
Star rotation rate	$14.^\circ71 d^{-1}$
Inclination of the Earth–Moon orbit	7°
Semimajor axis of the Earth–Moon orbit	1 au
Eccentricity of the Earth–Moon orbit	0.017
Longitude of the node of the Earth–Moon orbit	90°
Inclination of the Moon's orbit	10°
Semimajor axis of the Moon's orbit	384 000 km
Eccentricity of the Moon's orbit	0.055
Longitude of the node of the Moon's orbit	0°

in eccentricities and inclinations, whereas the differences between the full solutions and the standard precession rates increase more substantially. The period of $H(t)$ is also modified noticeably and the nutation in obliquity increases drastically by a factor of 40 for both satellites.

5.4 The Earth–Moon system

In this last example, we will consider the relativistic dynamics of the Earth–Moon system in orbit around the Sun. In this simplified model, the Earth–Moon system is considered as a point mass equipped with a spin equivalent in magnitude to the orbital angular momentum of the Moon's orbit around the Earth.[10] We take as reference plane the Sun's equatorial plane (so that the Sun's spin is aligned to the z-axis). The model of the Earth–Moon system as a Sun-orbiting gyroscope has been used to test the geodetic effect with high accuracy via lunar laser ranging measurements (Dickey et al. 1994; Williams, Newhall & Dickey 1996; Williams, Turyshev & Boggs 2004). The setup of our model is detailed in Table 12.

The pericentre precession in this system amounts to 3.836 arcsec century^{-1} without the Sun's spin and to 3.835 arcsec with the Sun's spin. The Lense–Thirring precession of the ascending node amounts to 0.33 mas century^{-1}. The 'spin' of the Earth–Moon system modifies the classical precession rates by a relative amount of about 10^{-6}. The period of $H(t)$ is 67.58 Ma, and the nutation in obliquity (which in this case is actually a nutation of the Moon's orbital inclination with respect to the inclination of the Earth–Moon system's orbit around the Sun) amounts to circa 6.5 arcsec. The instantaneous geodetic precession rate at $t = 0$ is about 1.9 arcsec century^{-1}, which is close to the experimental measure quoted by Will (2006) of 2 arcsec century^{-1}.[11]

We can observe how our results for this model agree with known results available in the literature. The time-scale in this system is quite long, due to the relatively large distance from the Sun, and, for the same reason, the modifications introduced by our solution over the classical results are rather small.

6 CONCLUSIONS AND FUTURE WORK

In this paper, we have presented for the first time a full solution for the angular coordinates in the averaged 1PN restricted two-body problem with spin. Our results, based on the theory of the Weierstrassian elliptic and related functions, take into account the full spin–orbit and spin–spin interactions, and they provide a smooth generalization of previous classical results which considered the various relativistic effects in isolation.

The application of our results to several idealized physical systems of interest highlights how the effects on the trajectory of the secondary body are, numerically, of order 1.5PN and higher (depending on the initial setup and the parameters of the system), and that they consist of periodic variations superimposed over a secular evolution of the angles. Similarly, the evolution in time of the spin vector of the secondary body is also quasi-periodic. Our solution highlights the existence of a periodic nutation in obliquity for the secondary body which, as far as we have been able to verify, has not been reported before.

Some of the idealized physical system that we have studied are at the limit of validity of our restricted model. The extension of our results to the full two-body problem, to be tackled in an upcoming publication, will allow us to study in detail systems – such as binary pulsars – that cannot be adequately described in the restricted case.

Another topic that will be a subject of future research is the use of our results to study the chaotic character of relativistic dynamical systems involving spinning bodies. This will be accomplished by incorporating higher order PN terms into the original Hamiltonian, which will then be subjected to multiple Lie transformations beyond the first order. The resulting transformed Hamiltonian will then be analysed to study aspects such as integrability, chaotic motion, resonances, etc. with standard techniques from Celestial Mechanics.

[10] The individual rotational spins of the Earth and the Moon are much smaller than the orbital angular momentum of the system, and they are thus ignored.
[11] In our model the parameters of the system are similar but not quite identical to those of the real Earth–Moon system.

ACKNOWLEDGEMENTS

The authors would like to thank the anonymous referee for useful suggestions that improved the manuscript.

REFERENCES

Abramowitz M., Stegun I. A., 1964, Handbook of Mathematical Functions: With Formulas, Graphs, and Mathematical Tables. Dover Press, New York
Arnold V. I., 1989, Mathematical Methods of Classical Mechanics, 2nd edn. Springer-Verlag, Berlin,
Aschenbach B., 2005, in Merloni A., Nayakshin S., Sunyaev R. A., eds, ESO Astrophysics Symposia, Growing Black Holes: Accretion in a Cosmological Context. Springer, Berlin, p. 302
Bailes M. et al., 2011, Science, 333, 1717
Baland R.-M., Yseboodt M., Hoolst T. V., 2012, Icarus, 220, 435
Barker B. M., O'Connell R. F., 1970, Phys. Rev. D, 2, 1428
Barker B. M., O'Connell R. F., 1975, Phys. Rev. D, 12, 329
Barker B. M., O'Connell R. F., 1976, Phys. Rev. D, 14, 861
Barker B. M., O'Connell R. F., 1979, Gen. Relativ. Gravit., 11, 149
Bills B. G., 2005, Icarus, 175, 233
Biscani F., Carloni S., 2013, MNRAS, 428, 2295 (Paper I)
Biscani F., Izzo D., 2014, MNRAS, 439, 810
Blanchet L., 2006, Living Rev. Relativ., 4, 9
Bogorodskii A. F., 1959, SvA, 3, 857
Cornish N. J., Levin J., 2002, Phys. Rev. Lett., 89, 179001
Cugusi L., Proverbio E., 1978, A&A, 69, 321
Damour T., 1987, in Hawking S. W., Israel W., eds, Three Hundred Years of Gravitation. Cambridge Univ. Press, Cambridge, p. 128
Damour T., 2001, Phys. Rev. D, 64
Damour T., Soffel M., Xu C., 1991, Phys. Rev. D, 43, 3273
Damour T., Jaranowski P., Schäfer G., 2008, Phys. Rev. D, 78, 024009
de Sitter W., 1916, MNRAS, 77, 155
Deprit A., 1969, Celest. Mech., 1, 12

Dickey J. O. et al., 1994, Science, 265, 482
Einstein A., 1916, Ann. Phys., Lpz., 354, 769
Einstein A., Infeld L., Hoffmann B., 1938, Ann. Math., 39, 65
Eisenhauer F. et al., 2011, The Messenger, 143, 16
Ford E. B., Joshi K. J., Rasio F. A., Zbarsky B., 2000, ApJ, 528, 336
Genzel R., Schödel R., Ott T., Eckart A., Alexander T., Lacombe F., Rouan D., Aschenbach B., 2003, Nature, 425, 934
Gibbons G. W., Vyska M., 2012, Class. Quantum Gravity, 29, 065016
Gradshteĭn I. S., Ryzhik I. M., 2007, Table of Integrals, Series, and Products. Academic Press, New York
Greenhill G., 1959, The Applications of Elliptic Functions. Dover Press, New York
Gurfil P., Elipe A., Tangren W., Efroimsky M., 2007, Regular Chaotic Dyn., 12, 389
Hackmann E., Lämmerzahl C., Kagramanova V., Kunz J., 2010, Phys. Rev. D, 81, 044020
Hartl M. D., Buonanno A., 2005, Phys. Rev. D, 71, 024027
Heimberger J., Soffel M., Ruder H., 1990, Celest. Mech. Dyn. Astron., 47, 205
Hoggatt V. E., 1955, Ph.D. dissertation, Oregon State College
Hori G., 1966, PASJ, 18, 287
Huang G., Ni X., Wu X., 2014, Eur. Phys. J. C, 74, 3012
Johansson F. et al., 2014, mpmath: A Python Library for Arbitrary-Precision Floating-Point Arithmetic (version 0.17). Available at: http://mpmath.org/
Kato Y., Miyoshi M., Takahashi R., Negoro H., Matsumoto R., 2010, MNRAS, 403, L74
Levin J., 2000, Phys. Rev. Lett., 84, 3515
Levin J., 2003, Phys. Rev. D, 67, 044013
Levin J., 2006, Phys. Rev. D, 74, 124027
Liu K., Wex N., Kramer M., Cordes J. M., Lazio T. J. W., 2012, ApJ, 747
Lorentz H. A., 1937, in Zeeman P., Fokker A. D., Nijhof M., eds, Collected Papers. Martinus Nijhoff, The Hague, Vol. 5
Lubich C., Walther B., Brügmann B., 2010, Phys. Rev. D, 81, 104025
Lyne A. G. et al., 2004, Science, 303, 1153
Mei L., Ju M., Wu X., Liu S., 2013, MNRAS, 435, 2246
Meyer L. et al., 2012, Science, 338, 84
Morbidelli A., 2002, Modern Celestial Mechanics: Dynamics in the Solar System, 1st edn. CRC Press, Boca Raton, FL
Morbidelli A., Giorgilli A., 1993, Celest. Mech. Dyn. Astron., 55, 131
Murray C. D., Dermott S. F., 2000, Solar System Dynamics. Cambridge Univ. Press, Cambridge
Sabha N. et al., 2012, A&A, 545, A70
Scharf G., 2011, J. Mod. Phys., 2, 274
Schiff L. I., 1960a, Am. J. Phys., 28, 340
Schiff L. I., 1960b, Proc. Natl. Acad. Sci. USA, 46, 871
Schnittman J. D., Rasio F. A., 2001, Phys. Rev. Lett, 87, 121101
Straumann N., 1984, General Relativity and Relativistic Astrophysics. Springer-Verlag, Berlin
SymPy Development Team 2014, SymPy: Python Library for Symbolic Mathematics. Available at: http://www.sympy.org
Tannery J., Molk J., 1893, Éléments de la Theorié des Fonctions Elliptiques. Vol. 4, Gauthier Villars Et Fils Imprimeurs, Paris
Thirring H., 1918, Phys. Z., 19, 33
Thomas P. C. et al., 1998, Icarus, 135, 360
von Zeipel H., 1916, Ark. Mat., Astron. Fys., 11, 1
Wex N., 1995, Class. Quantum Gravity, 12, 983
Whittaker E. T., Watson G. N., 1927, A Course of Modern Analysis, 4th edn. Cambridge Univ. Press, Cambridge
Will C. M., 2006, Living Rev. Relativ., 3, 9
Williams J. G., Newhall X. X., Dickey J. O., 1996, Phys. Rev. D, 53, 6730
Williams J. G., Turyshev S. G., Boggs D. H., 2004, Phys. Rev. Lett., 93, 261101
Wolszczan A., Frail D. A., 1992, Nature, 355, 145
Wu X., Xie Y., 2007, Phys. Rev. D, 76, 124004
Wu X., Xie Y., 2008, Phys. Rev. D, 77, 103012
Wu X., Xie Y., 2010, Phys. Rev. D, 81, 084045
Zhong S.-Y., Wu X., Liu S.-Q., Deng X.-F., 2010, Phys. Rev. D, 82, 124040

APPENDIX A: COMPUTING THE TIME OF ROOT PASSAGE

For this example, we will consider the case in which the polynomial $f_4(H)$ in equation (23) has four distinct real roots. The factorization of $f_4(H)$ can be written as

$$f_4(H) = C(r_0 - H)(H - r_1)(H - r_2)(H - r_3), \tag{A1}$$

where $C > 0$ is a scaling constant (so that the coefficient of H^4 is $-C < 0$) and r_i are the four real roots sorted in ascending order ($r_0 < r_1 < r_2 < r_3$). Topologically, this case corresponds to Fig. 1 (a): depending on the actual values of the initial conditions, the evolution of $\mathrm{d}H/\mathrm{d}t$ and H will be confined to one of the two libration lobes depicted in the figure.

We now assume that the initial value of $\mathrm{d}H/\mathrm{d}t$ (which can be computed from the initial conditions) is positive, and that the initial value of H is in the $[r_0, r_1]$ interval (i.e. the motion is confined to the left libration lobe). We choose, arbitrarily but without loss of generality, $H_\mathrm{r} = r_0$ as the value for H_r. It is then clear that t_r must be negative as H_r was reached before the initial value H_0,[12] and that the plus sign is to be chosen in equation (23) as the integration is to be performed in the upper half of the plane. We can thus rewrite the integral (23) as

$$\begin{aligned} t_\mathrm{r} &= \frac{1}{\sqrt{C}} \int_{H_0}^{H_\mathrm{r}} \frac{\mathrm{d}H}{\sqrt{(H_\mathrm{r} - H)(H - r_1)(H - r_2)(H - r_3)}} \\ &= \frac{-1}{\sqrt{C}} \int_{H_\mathrm{r}}^{H_0} \frac{\mathrm{d}H}{\sqrt{(H_\mathrm{r} - H)(H - r_1)(H - r_2)(H - r_3)}}, \end{aligned} \tag{A2}$$

where we have reversed the integration limits. This integral can be computed using a known formula (Gradshteĭn & Ryzhik 2007, section 3.147.2) as

$$t_\mathrm{r} = -\frac{2}{\sqrt{C(r_3 - r_1)(r_2 - H_\mathrm{r})}} F(\phi, k), \tag{A3}$$

where $F(\phi, k)$ is an incomplete elliptic integral of the first kind,

$$F(\phi, k) = \int_0^\phi \frac{\mathrm{d}\alpha}{\sqrt{1 - k^2 \sin^2 \alpha}}, \tag{A4}$$

and

$$\phi = \arcsin \sqrt{\frac{(r_3 - r_1)(H_0 - H_\mathrm{r})}{(r_1 - H_\mathrm{r})(r_3 - H_0)}}, \tag{A5}$$

$$k = \sqrt{\frac{(r_3 - r_2)(r_1 - H_\mathrm{r})}{(r_3 - r_1)(r_2 - H_\mathrm{r})}}. \tag{A6}$$

The generalization of this example to other cases is straightforward:

(i) if the integration is to be performed in the lower half of the plane because the initial value of $\mathrm{d}H/\mathrm{d}t$ is negative, a sign change is required;

(ii) if the integration is to be performed in the other libration lobe, the root r_2 can be chosen as H_r and the integral can be computed using the formula Gradshteĭn & Ryzhik (2007, section 3.147.6);

(iii) if the quartic polynomial has two roots, the integral can be computed using the formula Gradshteĭn & Ryzhik (2007, section 3.145.2).

[12] Strictly speaking, t_r can assume an infinite number of values, as $H(t)$ is a periodic function that assumes the value H_r an infinite number of times. By choosing as t_r the time of the last passage of $H(t)$ through H_r, the calculation of the integral (23) is greatly simplified.

As an alternative to the use of elliptic integrals in Legendre form, it is possible to compute the integral on the right-hand side of equation (23) directly using the inverse Weierstrass elliptic function $\wp^{-1}$ (see Whittaker & Watson 1927, section 20.6, and Hoggatt 1955).

APPENDIX B: CORRESPONDENCE BETWEEN SA VARIABLES AND SYMPLECTIC CYLINDRICAL SPIN VARIABLES

As mentioned in Section 2, the nature of the spin vectors in PN Hamiltonians has been a matter of debate in recent years. Whereas classical references (e.g. Barker & O'Connell 1975) express the PN Hamiltonians in a semi-Newtonian way in which the bodies are considered as rigid spinning spheres (to the point of including the kinetic energy terms of such rotating spheres in the Hamiltonian), other authors (such as Damour 2001) derive the Hamiltonians as classical limits of purely quantistic dynamical systems.

A key difference between these two approaches is that in the latter case (the 'quantum route') the equations of motion generated by the Hamiltonian for the spin variables are not Hamilton's equations. Indeed, the evolution in time of the spin vectors is given via a cross product involving the partial derivative of the Hamiltonian with respect to the spin vector itself (see equation 3.5 in Damour 2001). As noted in Wu & Xie (2010), the lack of symplecticity in the quantistic formulation can be an obstacle for certain types of applications (such as canonical perturbation theory and symplectic numerical integrators – see, e.g. Zhong et al. (2010) and Lubich, Walther & Brügmann (2010)).

In order to overcome this problem, Wu & Xie (2010) introduced a set of cylindrical-like coordinates for the spin variables, and they demonstrated that, in these coordinates, the Hamiltonian recovers a completely symplectic structure (while still satisfying the equations of motion derived via the quantum route). In the cylindrical coordinates of Wu & Xie (2010), the spins of the two bodies read

$$\boldsymbol{S}_i = \chi_i m_i^2 \hat{\boldsymbol{S}}_i, \tag{B1}$$

where the unit spin vectors are

$$\hat{\boldsymbol{S}}_i = \begin{pmatrix} \rho_i \cos\theta_i \\ \rho_i \sin\theta_i \\ k_i \xi_i \end{pmatrix}, \tag{B2}$$

θ_i are the longitudinal angles of the spin vectors, and

$$\rho_i = \sqrt{1-(k_i\xi_i)^2}, \tag{B3}$$

$$k_i = \frac{1}{\chi_i m_i^2}. \tag{B4}$$

In the Hamiltonian formulation, the θ_i play the role of generalized coordinates and the ξ_i are their conjugate momenta. Explicitly, the spin vectors read

$$\boldsymbol{S}_i = \left(\sqrt{\left(\chi_i m_i^2\right)^2 - \xi_i^2}\cos\theta_i, \sqrt{\left(\chi_i m_i^2\right)^2 - \xi_i^2}\sin\theta_i, \xi_i \right), \tag{B5}$$

where the $\chi_i m_i^2$ are the magnitudes of the vectors (which are conserved quantities) and ξ_i their z components.

We recall now from equation (8) that the components of the spin vectors in the SA formalism read

$$\boldsymbol{J}_i = \left(\sqrt{|\boldsymbol{J}_i|^2 - J_{i,z}^2}\sin\tilde{h}_i, -\sqrt{|\boldsymbol{J}_i|^2 - J_{i,z}^2}\cos\tilde{h}_i, J_{i,z} \right), \tag{B6}$$

where the $\tilde{h}_i$ are the nodal angles of the spins and play the role of generalized coordinates, and the z components $J_{i,z}$ are their conjugate momenta. In our Hamiltonian formulation, the magnitudes of the spin vectors $|\boldsymbol{J}_i|$ are also conserved quantities, due to the spherical symmetry of the bodies. It can be easily verified that the longitudes θ_i are geometrically related to the nodal angles $\tilde{h}_i$ by the simple relation

$$\tilde{h}_i = \theta_i + \frac{\pi}{2}. \tag{B7}$$

This is a trivial canonical transformation, and as such we can apply it directly to the coordinate $\tilde{h}_i$ to obtain the alternative symplectic formulation for $\boldsymbol{J}_i$:

$$\boldsymbol{J}_i = \left(\sqrt{|\boldsymbol{J}_i|^2 - J_{i,z}^2}\cos\theta_i, \sqrt{|\boldsymbol{J}_i|^2 - J_{i,z}^2}\sin\theta_i, J_{i,z} \right), \tag{B8}$$

which is clearly identical to (B5).

We have thus shown how our formulation of the spin variables in terms of SA elements is equivalent to the formulation of Wu & Xie (2010) in terms of cylindrical-like coordinates. Furthermore, this result establishes an interesting link between the semiclassical and quantistic formulations of the PN Hamiltonians with spin.

APPENDIX C: CODE AVAILABILITY

The PYTHON source code used to compute the results presented in this paper is available under an open-source license from the code repository: https://github.com/bluescarni/restricted_2body_1pn_angular.

This paper has been typeset from a TEX/LATEX file prepared by the author.